Chemotherapy resistance in CRISPR/Cas9-mediated *WEE1* knockout cells

Master of Science Thesis

Medicine with industrial specialization

(Biomedicine)

Author:

Issa Ismail Issa

1st of September 2018 – 31st of May 2019

AALBORG UNIVERSITY

AALBORG UNIVERSITY HOSPITAL

AALBORG UNIVERSITY

Project title: Chemotherapy resistance in CRISPR/Cas9-mediated *WEE1* knockout cells

Project period: 1st of September 2018 – 31st of May 2019

ECTS: 60

Supervisor:
Karen Dybkær, Professor
Department of Haematology, Aalborg University Hospital, Denmark

Co-Supervisors:
Johann Mar Gudbergsson, Ph.D. Fellow
Department of Health Science and Technology, Aalborg University, Denmark
Laboratory of Immunology & Cancer Biology

Hanne Due Rasmussen Ph.D. Fellow
Department of Haematology, Aalborg University Hospital, Denmark

Project group: 9048

Author:

Issa Ismail Issa,
Master of Science in Medicine with Industrial Specialization,
Master of Science Thesis, 9th and 10th semester.

Number of pages: 72

Acknowledgements

This master's thesis was developed during the 9th and 10th semester of my master's degree in Medicine with Industrial Specialization, Biomedicine. The experimental work was conducted from September 2018 to May 2019 in the Laboratory of Immunology and Cancer Biology at Aalborg University and the Department of Hematology at Aalborg University Hospital.

I would like to express my greatest acknowledgements to my main supervisor, professor Karen Dybkær, and my co-supervisors Johann Mar Gudbergsson and Hanne Due Rasmussen for their professional guidance throughout the entire project period. They have offered helpful advices, support, and motivation from the beginning.

I am very grateful to laboratory technicians Louise Hvilshøj Madsen and Helle Høholt for their instructions in the laboratory procedures and their technical assistance concerning puromycin selection, ddPCR and DNA purification.

A special thanks to Post Doc Alexander Schmitz for help with flow cytometry and associate professor Meg Duroux for giving me the opportunity conduct the experiments in the research laboratory. I would also like to thank my fellow student Daniel Lamdahl Justesen for assistance during laboratory procedures and relevant discussions concerning the study.

Table of contents

List of abbreviations

ABC	Activated B-cell-like
APC/C	Anaphase-promoting complex
BrdU	Bromodeoxyuridine
CAK	CDK-activating kinase
Cas9	CRISPR associated protein 9
CDS	Coding sequence
CHK1	Checkpoint kinase 1
CRISPR	Clustered regularly interspaced short palindromic repeats
crRNA	Crispr RNA
ddPCR	Droplet digital PCR
DLBCL	Diffuse large B-cell lymphoma
DMEM,	Dulbecco's modified Eagle's medium
DSB	Double strand break
E. Coli	Escherichia coli
eGFP	Enhanced green fluorescent protein
FBS,	Fetal bovine serum
GCB	Germinal-center B-cell–like
gDNA	Genomic DNA
GEP	Gene expression profiling
HBS	HEPES buffered saline
HEK	Human embryonic kidney
ICE	Inference of CRISPR Edits
Indel	Insertion or deletion
KO	Knockout
M-CDK	Mitosis promoting CDK complex
miR	Micro RNA
MOI	Multiplicity of infection
NMD	Non-sense mediated mRNA decay
NoRT	No-reverse transcriptase
Oligo	Oligonucleotide
P/S	Penicillin/streptomycin
PAM	Protospacer adjacent motifs
PBS,	Phosphate buffered saline
PCR	Polymerase chain reaction
PI	Propidium iodide
PL	Plasmid control
PLK1	Polo-like kinase 1
PTC	Premature termination codon
R-CHOP	Rituximab, Cyclophosphamide, Doxorubicin, Vincristine (Oncovin) and Prednisolone

RPMI	Rosewell park memorial institute
RT	Room temperature
SAC	Spindle-assembly-checkpoint
sgRNA	Single guide RNA
siRNA	Small interfering rnas
TALEN	Transcription activator-like effector nucleases
TBP	TATA-box binding protein
tracrRNA	Trans-activating crrna
UTR	Untranslated region
WT	Wild type
ZFN	Zinc-finger nucleases

Abstract

Background: Diffuse large B-cell lymphoma (DLBCL) is an aggressive and highly heterogenous type of cancer. Despite receiving the standard combination immunochemotherapy, 40% of patients die due to relapsed disease. The mechanisms controlling treatment response are not fully elucidated and require more experimental dissection. Inhibition of WEE1 protein results in abrogation of the G2/M phase transition of the cell cycle, and this has been shown to potentiate the cytotoxic effects of antimitotic drugs used in DLBCL treatment, such as vincristine.

Hypothesis: We hypothesize that *WEE1* plays an important role in drug resistance in DLBCL. By using the CRISPR/Cas9 technology a *WEE1* gene knockout can be induced, whereby we can gain important insight into the role of *WEE1* in vincristine resistance in DLBCL.

Methods: Four sgRNAs targeting *WEE1* were designed and cloned into CRISPR/Cas9 plasmid vectors alongside a non-targeting sgRNA. Cloning was verified by PCR and Sanger sequencing, and plasmids were transfected into HEK293T cells to induce a knockout of *WEE1*. The ICE tool was utilized to assess the editing and knockout efficiencies for each sgRNA. Basic characterization was done on bulk *WEE1* knockout cells, including cell proliferation, cell cycle analysis, and droplet digital PCR. In addition, functional assays consisting of vincristine drug screens were conducted to assess the role of *WEE1* in vincristine sensitivity.

Results: Transfection with the sgRNA containing plasmid constructs successfully induced insertion and deletion mutations in *WEE1*. Transfected cells reduced proliferation rate, however no change in the cell cycle could be observed. In addition, ddPCR indicated an increase in *WEE1* mRNA expression. Despite using heterogenous cell populations, a significant growth inhibition was observed in some of the *WEE1* knockout cells after treatment with vincristine, and this corresponded to the *WEE1* editing and knockout efficiencies.

Conclusion: The findings from this study suggest that knockout of *WEE1* holds great potential in sensitizing DLBCL cells to vincristine.

Dansk Resumé

Baggrund: Diffust storcellet B-celle lymfom (DLBCL) er en aggressiv og heterogen kræfttype. Til trods for behandling dør omkring 40% af patienter grundet sygdomstilbagefald. Disse patienter har en resistens mod kombinationsbehandlingen, og de underliggende mekanismer herfor endnu ikke er klarlagt. Inhalering af WEE1 proteinet, som kontrollere overgangen til mitosen, har vist sig øge effekten af antimitotiske midler, herunder vincristin.

Hypotese: Vores hypotese er at *WEE1* spiller en væsentlig rolle i DLBCL behandlingsresistens og ved at bruge CRISPR/Cas9 teknologien kan gene slukkes, hvorved vi kan herved få et vigtigt indblik herfor.

Metoder: Fire sgRNAer blev designet til at targetere *WEE1* genet og klonet in i CRISPR/Cas9 sammen med et ikke-targeterende sgRNA. Kloningen blev verificeret ved PCR og Sanger sekventering, og plasmiderne blev dernæst transfekteret til HEK293T celler for at inducere en slukning af *WEE1* genet. For at vurdere redigeringseffektiviteten af alle sgRNA blev ICE værktøjet udnyttet. Der blev udført karakteriserende eksperimenter af de transfekterede, heterogene celle kulturer med *WEE1* knockout herunder celle proliferation, celle cyklus analyse og ddPCR eksperimenter. Slutteligt blev der også udført funktionelle eksperimenter som bestod af Vincristin dosis respons forsøg af de transfekterede celler, for at vurdere rollen af *WEE1* i forhold til vincristin sensitiviteten.

Resultater: Transfektion med plasmider som indeholdt sgRNAer inducerede alle mutationer bestående af insertioner og deletioner af *WEE1* genet. Vækstraten var lavere for de transfekterede celler, men der var ingen ændring i cellecyklus. ddPCR indikerede til gengæld en højere ekspression af *WEE1* mRNA. Selvom der blev brugt heterogene celle populationer med *WEE1* knockout, kunne der stadig ses en signifikant vækstinhibering i nogle af cellerne efter behandling med vincristin. Disse stemte overens med gen redigerings- og knockout effektiviteten.

Konklusion: Dette studie indikerer at en slukning af *WEE1* genet kan øge DLBCL cellers sensitivitet ved vincristin behandling.

1. Introduction

Lymphomas are a group of hematological cancers originating from malignant lymphocytes of natural killer cells, T-cells, or B-cells and are classified based on their cell-of-origin, morphology, immunophenotype, and genetic aberrations (1). Formation of lymphoma is characterized by the usual hallmarks of cancer including sustained proliferative signaling, evasion of growth suppressors, activation of invasion and metastasis, replicative immortality, angiogenesis, and resistance to apoptosis in addition to reprogrammed energy metabolism and evasion of the immune system (1,2). These traits are acquired due to genetic and epigenetic modification in a multistep process towards dysregulation of several genes ultimately resulting in malignancy (1,2). The two main classes of lymphoma are Hodgkin's Lymphoma and Non-Hodgkin's Lymphoma, with the latter being the most prominent accounting for approximately 90% of cases (3).

1.1 Diffuse large B-cell lymphoma

Diffuse large B-cell lymphoma (DLBCL) is the most frequent lymphoid neoplasm among adults constituting 30-40% of Non-Hodgkin's Lymphoma cases and every year approximately 450 new patients are diagnosed in Denmark (4,5). It is most prevalent in adults, with a median age in the 7th decade where most patients present with a rapidly growing tumor mass involving one or more lymph nodes, while 40% also present with extranodal involvement (6). Approximately one third of patients display typical B symptoms constituting night sweats, fever, and weight loss in addition to symptoms related to organ involved (4,6). The etiology of most DLBCL cases remains unknown. Despite this, distinctions are still made between cases where tumors arise de novo (referred to as a primary disease) and other less common cases where they arise from progression or transformation of indolent lymphomas or leukemias (referred to as secondary disease) (4).

1.1.1 Subclassifications of DLBCL

DLBCL is both biologically and clinically heterogenous. The heterogeneity of DLBCL is reflected in the many attempts at subclassification of the disease. Both preclinical and clinical studies have proposed subdivisions based on histological variants, molecular and immunophenotypic subclasses, as well as clinical parameters included in the International Prognostic Index (IPI; e.g. age, extranodal sites, performance status, Ann Arbor stage and serum lactate dehydrogenase levels) (4,7).

One of the most common methods for subclassifications of DLBCL is based on gene expression profiling (GEP) where thousands of genes are simultaneously assessed through DNA microarray (8).

This has led to the creation of DLBCL subclasses based on cell-of-origin gene signatures, which reflect normal B-cell from peripheral blood activated in vitro and germinal center B-cells (8). The two subclasses are activated B-cell-like (ABC) and germinal-center B-cell–like (GCB). In addition a smaller unclassifiable subgroup also exists (1,8). The two subgroups are both molecularly and clinically distinct, and differ by the expression of more than 1000 genes, in gene activation mechanisms, genetic aberrations, and clinical outcome after treatment (8,9).

1.1.2 Treatment of DLBCL

DLBCLs are aggressive but potentially curable. The standard first-line treatment in DLBCL is a combination immunochemotherapy consisting of cyclophosphamide, doxorubicin, vincristine, and prednisolone combined with the monoclonal anti-CD20 antibody, rituximab (R-CHOP). Treatment results in overall 5-year survival rates of 60-70% in patients depending on their risk-profile (6). The prognosis of R-CHOP treated patients is better for the GCB subtype compared to the more aggressive ABC subtype (10,11). Despite an increase in overall survival with the addition of rituximab to the standard therapy (10), 30-40% of patients remain or become resistant to treatment (11). The molecular mechanisms behind treatment resistance is still not fully understood, and multiple biological agents targeting biomarkers and signaling pathways of DLBCL have been combined with R-CHOP with limiting success (12,13).

Vincristine (O, Oncovin) has been widely used as an anticancer drug for over 50 years (14). It is an antimitotic drug which binds to tubulin, whereby tubulin dimers can no longer polymerize and form the mitotic spindle microtubules (15). This inhibits the progression from metaphase during the cell cycle as chromosomes cannot be separated (15). Consequently, cell proliferation is decreased in a vincristine concentration dependent manner, where antiproliferative effects are seen at low concentrations and deterioration of microtubule organization is initiated as concentration increases (16).

1.1.3 Biomarkers related to oncogenic pathways in DLBCL

Several biomarkers have been observed in DLBCL and associated with disease outcome. The most robust single marker is *MYC*, which is expressed in 10-15% of all DLBCL cases. Expression or amplification of *MYC* worsens the prognosis and results in poor overall survival. MYC-positive patients often co-express BCL2 protein and translocation mutations in both of these genes (known as double hit lymphoma) results in dismal prognosis, even when using very high doses of chemotherapy. (11,17,18)

Generally, mutations in checkpoint proteins are frequent in all cancer types. The tumor suppressor protein p53, which functions by inducing cell cycle arrest or apoptosis in the case of DNA damage, is known to be the most commonly mutated gene in human cancers (19,20). In DLBCL, mutation in the p53 gene can be found in 18-24% of cases and is associated with poor prognosis in R-CHOP treated patients (21,22). Moreover, p53 gene mutations can be used to stratify GCB-DLBCL patients into distinct subsets with different overall survival (21). In addition, mutations can be found in genes and pathways related to chromatin modifications, B-cell lineage commitment, nuclear factor-kappa B, and WNT signaling among others, reflecting the genetic molecular heterogeneity of in DLBCL. Improved insight and biological understanding of the activations of these oncogenic pathways and how they affect cell growth could offer better targeted therapies for patients resistant to standard therapy. (23,24)

As one of the fundamental aspects in the hallmarks of cancer is deregulated growth caused by aberrant activity of cell cycle proteins, cancer therapies targeting cell cycle regulators offer great therapeutic potential and various cell cycle inhibitors such as WEE1 inhibitors are currently used in clinical trials (2,25).

1.2 WEE1 kinase as a target for cancer therapy

To understand the mechanism of action for chemotherapeutic drugs targeting cell cycle proteins and their importance in cancer therapy, it is essential to first understand cell cycle regulation.

1.2.1 The WEE1 pathway

Progression through the cell cycle is monitored and tightly regulated by cell cycle checkpoints, and at the G2/M checkpoint, WEE1 plays an essential role. WEE1 is a nuclear kinase that negatively regulates cell cycle progression at the G2/M phase transition (26,27). The protein is encoded by the *WEE1* gene located on chromosome 11 (at locus 11p15.3-p15.1) (28) and is expressed as two protein isoforms produced by alternative splicing of the transcript (29).

WEE1 regulates the entry into the M-phase by inactivating the mitosis promoting CDK complex (M-CDK; comprised of cyclin B and CDK1) through inhibitory phosphorylation at its ATP-binding site. As M-CDK is responsible for both entry into mitosis as well as successful completion of mitosis this inactivation results in cell cycle arrest at the G2/M checkpoint. Complete activation of M-CDK is dependent on; binding to cyclin B, activating phosphorylation by CDK-activating kinase (CAK), and removal of WEE1 induced inhibitory phosphate groups by the phosphatase, Cdc2 (figure 1A). Once

activated it engages in a positive feedback loop inhibiting WEE1 while activating Cdc25, enforcing additional activation (30,31).

M-CDK initiates transition to M-phase through phosphorylation of a large variety of substrates. In short, the phosphorylation of M-CDK substrates results in: initiation of sister chromatid condensation, spindle assembly in early mitosis along with polo-like kinase 1 (PLK1), the attachment of sister chromatids to the spindle mediated by Aurora B kinases, nuclear envelope breakdown, rearrangement of Golgi apparatus and cytoskeleton among other mechanisms in early mitosis (figure 1B). (31,32) Once the cell reaches the metaphase-to-anaphase transition during mitosis, the anaphase-promoting complex or cyclosome (APC/C; a ubiquitin ligase that initiates proteolytic destruction of several proteins) becomes a key regulator of mitosis and eventually leads to mitotic exit. The spindle-assembly-checkpoint (SAC) proteins ensure that APC/C is not activated until all microtubules are properly attached to the sister chromatids and chromosomes have been aligned appropriately for successful separation and thereby progression from metaphase to anaphase. (33,34)

However, these events can only occur if the cell passes the G2/M checkpoint. DNA damage obtained throughout the cell cycle causes an activation of the G2/M checkpoint, where cell cycle progression is halted to recover damage (32). Upon recognition of DNA damage, the checkpoint kinase 1 (CHK1) is activated and induce G2 checkpoint arrest by phosphorylating Cdc25, whereby the M-CDK becomes inactive since the WEE1-mediate phosphate groups cannot be removed. This is further enforced by CHK1 mediated activating phosphorylation of WEE1, leading to further inactivating phosphorylation of M-CDK and thus enforcing G2 arrest. (35)

Once DNA damage is recovered, the cell cycle can continue, and the cell is ready to enter mitosis. Here, active M-CDK complexes phosphorylate WEE1, which initiates a cascade leading to WEE1 degradation thus ensuring WEE1 activity is suppressed during mitosis. This further amplifies M-CDK activation, and contribute to the early mitotic events. (32,36,37)

A)

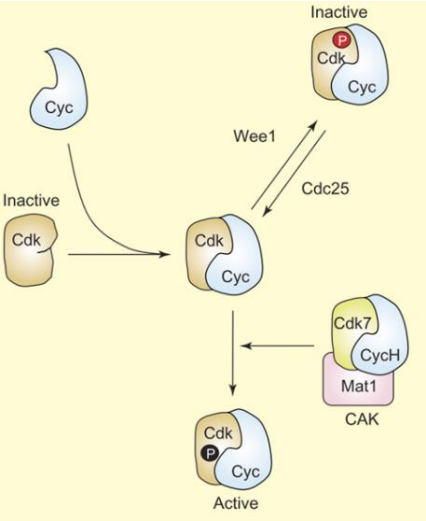

B)

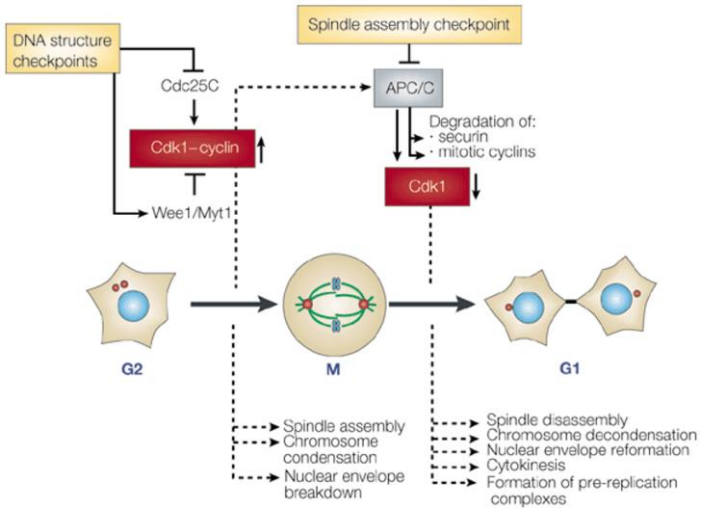

Figure 1). **The role of WEE1 during the cell cycle**. (**A**) **WEE1 functions by inactivating M-CDK (CDK1 and cyclin B complex)**. In order to be activated, CDKs require binding to cyclins. CDK-cyclin complexes such as M-CDK can be activated through activating phosphorylation in the T-loop region mediated by CAK. In contrast, they can be negatively regulated through inhibitory phosphorylation by WEE1, and these inhibitory phosphate groups can be removed by Cdc25 phosphatase whereby the complexes are activated. Figure modified from (38). (**B**) **The main events during the last two phases of the cell cycle.** WEE1 activated through phosphorylation, whereby it can inhibit the M-CDK complex during the G2/M checkpoint to ensure genomic stability prior to mitosis. Once the cell is ready to enter mitosis, WEE1 is inactivated and the inhibitory phosphate groups on M-CDK are removed by Cdc25. Hereby the cell enters the M-phase, and the early events of mitosis are initiated. Once the spindle assembly checkpoint is passed, APC/C is activated, and mitosis can be completed. Figure is obtained from (31).

1.2.2 Dysregulation of WEE1

Cells lacking functional WEE1 proteins enter mitosis prematurely at the expense of genomic integrity due to the inability to arrest cells at the G2/M checkpoint (39–41). In fission yeast, aversion of the G2/M checkpoint due to WEE1 loss results in cell division before the critical size for cell cycle progression is achieved, resulting in smaller daughter cells than normal, in contrast to the delayed mitosis entry and greater size observed in WEE1 expressing cells (40). WEE1 mutant cells exhibit several mitotic abnormalities such as disorganized and multipolar spindles, chromosomal misalignment and lagging chromosomes during anaphase. This contributes to deregulated mitosis, whereby the mutant cells progress through mitosis at the expense of genomic integrity. Additional findings include mitotic exit without cytokinesis and prolongation of mitosis without completion which might lead to extrachromosomal DNA and polyploidy seen in *WEE1* deficient cells. (42)

In addition to defective cell division in the absence of WEE1, increased expression of WEE1 can also lead to detrimental consequences in cells (43). High expressions of *WEE1* mRNA was found in DLBCL patient specimen, and was significantly higher in the GCB subtype compared to the ABC and unclassified subtypes (44). Overexpression of *WEE1* has also been observed in adult acute

lymphoblastic leukemia samples (45). In malignant melanoma increased expression of *WEE1* was associated with malignancy and poor disease-free survival supporting the claim that WEE1 has a tumor promoting role, and can serve as a prognostic biomarker (46). Increased *WEE1* expression have similarly been observed in a large variety of other human cancers (43).

In contrast to the tumor promoting role of *WEE1*, a dual role as a tumor suppressor has also been described where loss of WEE1 might inadvertently promote the accumulation of genetic aberrations in pre-neoplastic lesions (45). This might explain the underexpression of *WEE1* seen in colon-, prostate-, and non–small cell lung cancer cells, as loss of *WEE1* induces genetic aberrations in the pre-neoplastic tissues, thus promoting carcinogenesis (43,47–49). Conversely, cells that already have genomic instability, and typically also defective G1 checkpoint due to deficits in p53 signaling, rely on WEE1 for survival. Hereby, *WEE1* functions as a conserving oncogene and serves as a potential target for DNA damaging therapy. (43,50)

1.2.3 Targeting WEE1 through inhibition

Multiple studies have taken advantage of the deficient G1-arrest and dependency of the G2/M checkpoint of cancer cells by using WEE1 inhibitors to overcome the G2/M checkpoint and push the cells into mitosis prematurely. This premature M-phase entry of cells with genomic instability elicits mitotic catastrophe and subsequent cell death by apoptosis after significant DNA damage, and has therefore been suggested as a means of killing cancer cells. (51–54)

In B-cell lymphomas, inhibition of WEE1 has been shown to significantly enhance apoptosis of G2 phase-arrested cells, through the induction of premature entry into mitosis and mitotic catastrophe (52). Similar observations has been made in glioblastoma, where WEE1 inhibition caused mitotic catastrophe and apoptosis in primary cells (55). In an array of cancer cells with aberrant G1-checkpoint, WEE1 inhibition resulted in abrogation of G2 checkpoint, and sensitized the cells to DNA damage caused by irradiation or topoisomerase inhibition. In addition, cytotoxicity was more pronounced in p53 deficient cells, keeping up with the idea, that cancer cells with deficient G1 checkpoint are more sensitive to G2 checkpoint abrogation by WEE1 inhibition. (56,57)

Moreover, great potential has been shown when combining WEE1 inhibition with immune- and chemotherapeutic drugs (54). A major challenge in resistance to antimicrotubule drugs is SAC slippage. These drugs activate the SAC by targeting microtubules and obstructing mitotic spindle assembly and thereby delay mitosis exit and promote apoptosis (34,58). Genetic and chemical WEE1 inhibition has been shown to strengthen the SAC, extend mitosis, and potentiate killing through

increased apoptosis when used in combination with vincristine in acute lymphoblastic leukemia cells (58). Additionally, combining WEE1 inhibitors with rituximab has been shown to result in additive cytotoxicity both rituximab sensitive and rituximab insensitive DLBCL cell lines (44). Similarly, when combining WEE1 inhibitors with doxorubicin in DLBCL cell lines significantly increased cell killing (57).

WEE1 has also been identified as a potential therapeutic target in largescale RNA interference screenings of cervical, breast and lung cancer cell lines (59,60). In addition, small interfering RNA (siRNA)-induced downregulation of *WEE1* has been shown to completely abolish mitotic exit in Cdc20-depleted (and thereby APC/C defective) cells (37).

Most of the abovementioned studies using WEE1 inhibitors, have used the agent MK-1775 (also known as AZD1775). This is a small molecule potent WEE1 inhibitor used in clinical trials and in studies investigating the biology of *WEE1* (54). However, it has recently been found that it also target PLK1 with a similar potency, thus indicating that MK-1775 is actually a dual WEE1 and PLK1 inhibitor, which limits its use as a specific drug for WEE1 inhibition. (61) To investigate the role of WEE1 in cancer, other agents must be utilized for chemical inhibition of WEE1. Alternatively, small interfering RNAs (siRNAs) have also been used to inhibit *WEE1* through the induction of gene knockdown, but since these regulate gene expression post-transcriptionally, WEE1 protein have been detected after siRNA treatment (61). Induction of a gene knockout is therefore more favorable to completely disrupt WEE1 production, and this has been demonstrated previously by using the CRISPR/Cas9 system (61).

1.3 The CRISPR/Cas9 system

CRISPR/Cas9 is a new efficient genome editing tool adapted from the prokaryotic immune system. It is a two-component system consisting of CRISPR (Clustered Regularly Interspaced Short Palindromic Repeat) and the Cas9 (CRISPR associated protein 9) endonuclease. CRISPR was initially discovered as DNA sequences in the genome of E. Coli (62), and the function was later described as a defense mechanism against bacteriophages (63). In prokaryotic cells, adaptive immunity is acquired through the CRISPR-Cas system by first sampling pieces of foreign genetic elements (i.e. plasmids or bacteriophages) from sites referred to as protospacer regions that are juxtaposed to short recognition sequences called protospacer adjacent motifs (PAM) (figure 2A). These are incorporated into the CRISPR loci in the genome of the cells as new spacer sequences, where they are separated by short palindromic repeats. (63,64) During expression stage, both

sequences are transcribed into pre-crRNAs, processed, and expressed as interfering CRISPR RNAs (crRNAs) that contains the spacer sequences. Lastly, during the interference stage they assemble into Cas endonucleases and direct them to sequence-specific target sites (the protospacer sequences) located upstream of the PAM, whereby Cas induces double stranded breaks (DSB) the foreign DNA leading to its degradation. (65) There are many CRISPR–Cas systems in nature, that use different Cas endonucleases that require different PAM sequences for DNA cleavage. *Streptococcus pyogenes* Cas9 endonuclease (spCas9) remains the best characterized and requires a 5'-NGG PAM sequence (65). By utilizing this bacterial defense mechanism and repurposing it through modifications, a powerful and programmable tool for precise gene editing has been developed. (66)

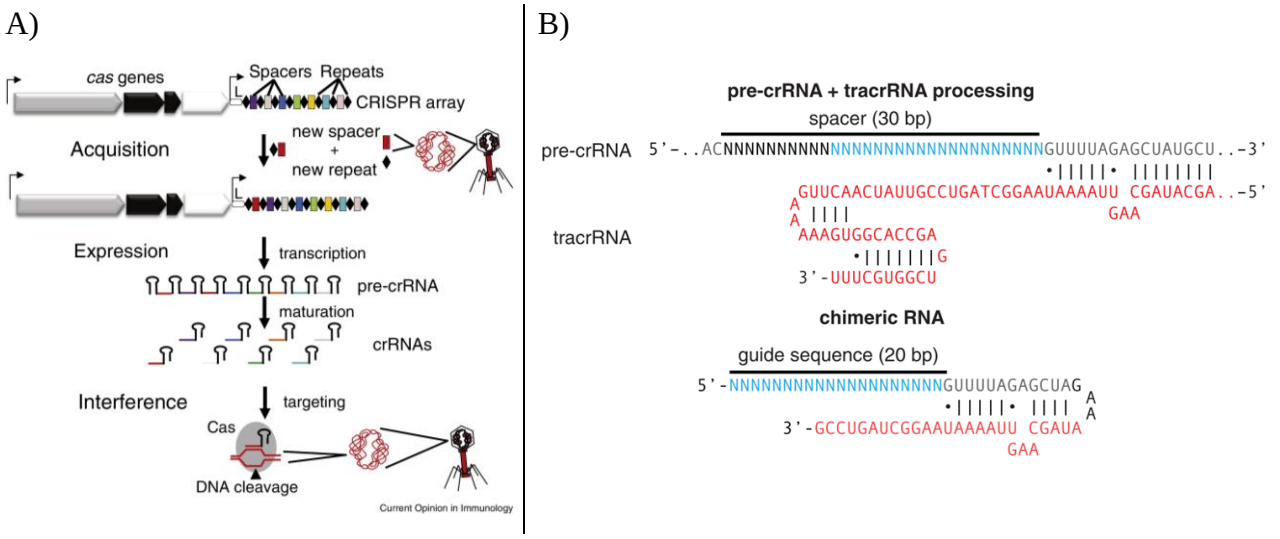

Figure 2) (**A**) The CRISPR-Cas immune system in prokaryotic cells (65). (**B**) The pre-crRNA:tracrRNA complexes (top) and the engineered chimeric RNA which only uses a 20 nt spacer sequence (bottom) (67).

There are three major CRISPR/Cas systems (type I, II, and III), and the main difference occurs in the processing of pre-crRNAs (68). For genome editing, the type II system which uses spCas9 has been utilized. This system uses two short RNA molecules: the crRNA and a trans-activating crRNA (tracrRNA), that are complementary to the repeat sequences in crRNA. TracrRNA acts as a scaffold which links crRNA to Cas9 in addition to facilitating the pre-crRNA maturation. In 2012, by fusing fused these two RNAs into a single, chimeric tracrRNA:crRNA molecule termed single guide RNA (sgRNA), it was discovered that SpCas9 can be reprogrammed to target multiple genomic loci (figure 2B). The sgRNA structure maintains a 20 nucleotide (nt) sequence at the 5' end of the molecule which is complementary to the target protospacer site juxtaposed to the PAM sequence, and a the tracrRNA which forms a scaffold that binds to Cas9. (66,69,70) Targeted gene editing can hereby be accomplished by redesigning the 20 nt spacer (the sequence specific part of the sgRNA) to target any

desired site in the genome (figure 3). The main restriction is the requirement of a 5'-NGG PAM sequence for spCas9 which occurs at every 8 bp on average throughout the human genome. (67)

Once the complex is binds to the putative target sequence with sufficient homology, Cas9 will induce a double strand break (DSB) 3 bp upstream of the PAM sequence, which is then repaired by one of two repair pathways. The most common repair pathway is the error prone non-homologous end joining (NHEJ), which often introduce insertion or deletion mutations (indels) around the Cas9 cut site that can disrupt the coding sequence of targeted genes by the formation of a premature stop codon. The second pathway is homology directed repair (HDR), which requires a donor template (e.g. a sister chromatid) to repair the DSB. (71,72)

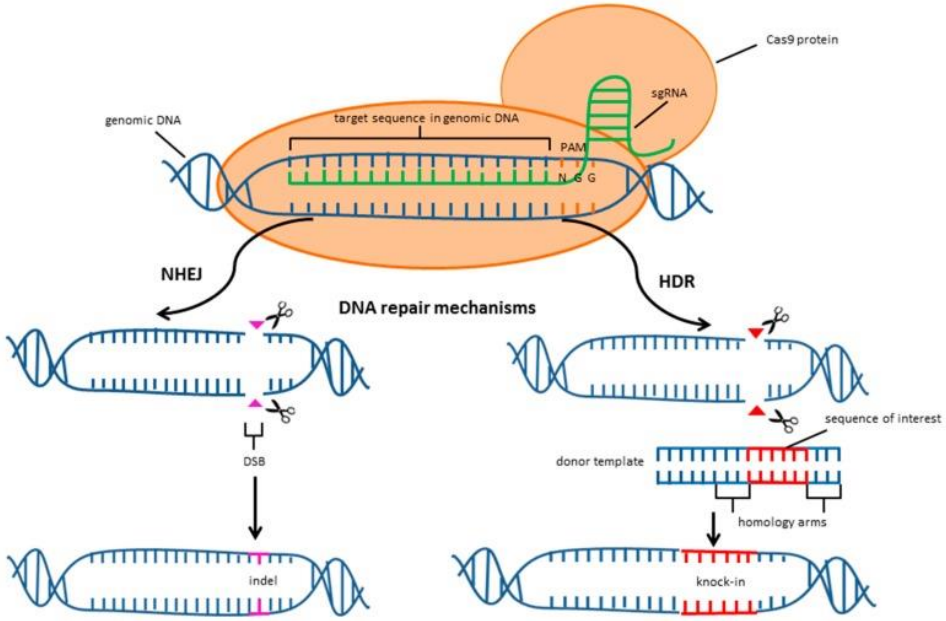

Figure 3) **Illustration of the CRISPR/Cas9 system**. CRISPR/Cas9 is a two-component genome editing tool, consisting of Cas9 endonuclease and a sgRNA complementary to the desired target sequence. Once the complex binds to the target sequence, Cas9 induces a DSB, which is most commonly repaired trough the NHEJ repair pathway, or alternatively the HDR repair pathway. Figure is obtained from (73).

The predecessors for this technology was the zinc-finger nucleases (ZFNs) and transcription activator-like effector nucleases (TALENs) genome editing tools which were based on the DNA-protein recognition. However difficulties in the synthesis and validation of new pairs of nuclease proteins with varying sequence specificity for every genomic target complicated the routine use of these engineered nucleases (74). In contrast, CRISPR/Cas9 is more simple and adaptive, as Cas9 specificity relies on the interaction between the sgRNA and the target site. (75)

Currently there are three main editing strategies when using CRISPR/Cas9. The first one is the plasmid-based approach where the genes encoding Cas9 and CRISPR are delivered in the same vector

whereby multiple transfections are avoided (76). The second strategy is the mRNA based one, where sgRNA is delivered into the cell along with Cas9 mRNA (77). In the last strategy, the entire CRISPR/Cas9 ribonucleoproteins at once (78,79). The plasmid-based approach is the most straight forward method. Here as a single transfection is required to express both the sgRNA and Cas9 protein at once, making it a simple and convenient. In addition it also offers greater stability than the mRNA based approach, and does not require the synthesis of ribonucleoproteins prior to gene editing. (80)

A large variety of CRISPR/Cas9 delivering strategies exists. Transfection of cells can be achieved using chemical or physical methods such as calcium phosphate transfection, electroporation and lipids, and are relatively simple in many *in vitro* cell lines. However, when working with hard-to-transfect cells or *in vivo* experiments, direct delivery using these methods is often insufficient. In these cases, transduction through viral particles such as lentiviral, offers a better alternative, and has widely been used as gene vehicles. (81) Through lentiviral transduction, large packages can be delivered with great efficiency, and long term (stable) gene expression can be achieved by integration of the transgene into the host genome of both dividing and non-dividing cells (80,82). Despite the potential risk of insertional mutagenesis, lentiviral vectors offer great potential for gene therapy and have been approved for clinical studies (80,83,84).

1.4 MiR-155 targets WEE1 and controls vincristine sensitivity

By using lentiviral transduction of DLBCL cell lines and the CRISPR/Cas9 system, the effects of vincristine resistance have previously been investigated (85). Here, micro RNA 155 (miR-155) was transduced into two GCB-DLBCL cell lines; SU-DHL-5 which is vincristine sensitive, and OCI-Ly7 which is resistant to vincristine. miR-155 transduction induced vincristine sensitivity in OCI-Ly7, and targeted gene analysis based on miR-155-mRNA interactions revealed that *WEE1* was a target of miR-155, suggesting that *WEE1* expression could play a role in the increased vincristine sensitivity observed. In line, experiments revealed an increase in WEE1 protein expression in CRISPR/Cas9-mediated miR-155 knockout cells, and experiments using WEE1 chemical inhibition showed increased sensitivity to vincristine, demonstrating that *WEE1* is an excellent candidate target in vincristine resistant DLBCL. (85)

1.5 Hypothesis, aim, and objectives

DLBCL is the most common type of lymphoma, and despite receiving the standard R-CHOP combination therapy, up to 40% of patients die due to relapse or refractory disease (11). Subclassification of DLBCL into different molecular subtypes have identified biomarkers and underlying drug response and resistance mechanisms supporting the strategy of better risk stratification of patients. However, the mechanisms controlling treatment response are not fully elucidated and require more experimental dissection and most likely specific subclassification attention.

Cancer cells, including DLBCL, often have deficient G1-arrest and thus rely more on the G2/M checkpoint where *WEE1* plays a crucial role for their survival (43,50). The G2/M checkpoint has been abrogated in previous studies by both genetic and chemical inhibition of WEE1 protein. This has resulted in genomic instability and significant DNA damage, leading to increased rates of apoptosis (42,58). Combining this with anti-mitotic drugs such as vincristine has enhanced this effect. Recently, it was shown that genetic manipulation of miR155 impacts the levels of *WEE1* in vincristine-resistant GCB-DLBCL cells, and downregulation of WEE1 sensitized these cells to vincristine treatment (85).

Based on these findings, the main hypothesis in this study is that *WEE1* plays an important role in drug resistance in DLBCL. By targeting *WEE1* using CRISPR/Cas9 technology to induce a gene knockout, we might gain important insight into the biological role of *WEE1* in vincristine resistance in DLBCL and obtain a model system where we can possibly reverse drug resistance.

The overall aim was therefore to unravel the role of *WEE1* in vincristine response in DLBCL. This was pursued through the following main objectives, where the HEK293T cell line was used as proof-of-concept for *WEE1* gene editing and subsequent characterization and functional assays:

I. Generation of CRISPR/Cas9 plasmid constructs targeting *WEE1* by designing sgRNAs, cloning these into plasmids, and verification of correct insertion.
II. Lentiviral production and determination of transfection/transduction efficiencies of HEK293T and OCI-Ly7 cells
III. Generation of *WEE1* knockout cells and determination of editing and knockout efficiency for each sgRNA in heterogenous cell populations.
IV. Characterization and functional assays of knockout cells, including cell cycle analysis, droplet digital PCR, and vincristine drug response assays.

2. Materials and Methods

The experimental workflow and methods in this project are summarized in figure 4.

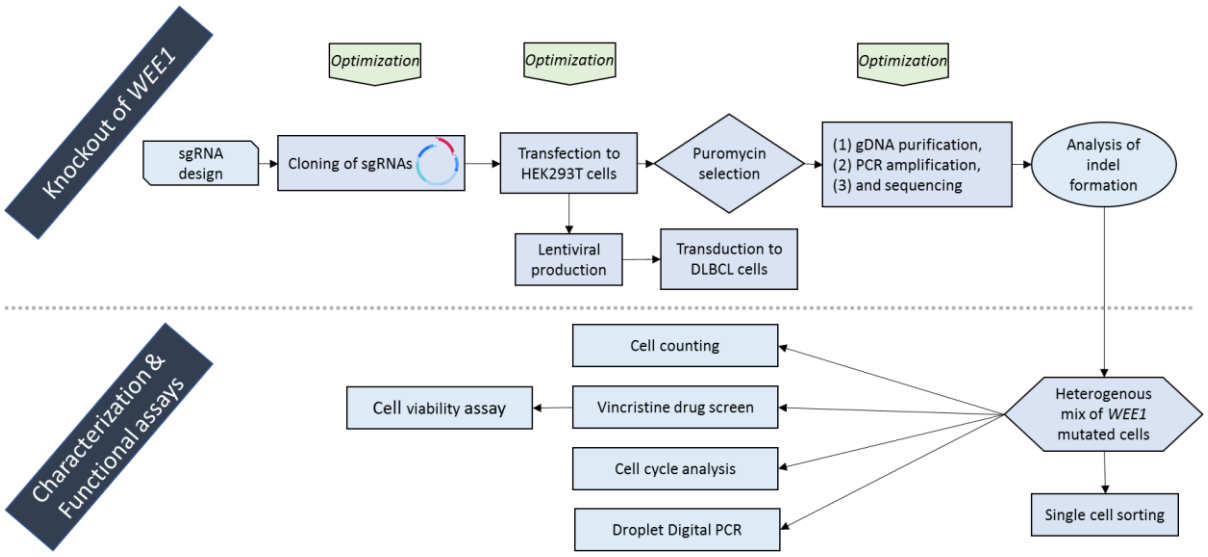

Figure 4) **Flowchart providing an overview of the experimental workflow in this project**. First, experiments leading to *WEE1* knockout in HEK293T cells were initiated by sgRNA designing candidate sgRNA. These were cloned into a plasmid backbone and transfected into HEK293T cells. Subsequently, transfected cells were puromycin selected, a region surrounding the CRISPR/Cas9 cut site was PCR amplified, and editing efficiency was analyzed by Sanger sequencing and use of online tools. Next, characterization and functional assays were conducted in the heterogenous mix of transfected HEK293T cells. These included: cell counting, cell cycle analysis, droplet digital PCR, and a vincristine dose-response assay.

2.1 Single guide RNA design

Four sgRNAs targeting exon 2 in *WEE1* were designed using the human Genome Reference Consortium Human Build 38 (GRCh38) as a reference genome and the PAM fitting the spCas9 endonuclease. The online software tools CrispOR (86) and CHOPCHOP (87) were utilized to achieve this. sgRNAs with the highest predicted specificity and efficiency scores in combination with the lowest off-target scores were selected (figure 5A). Furthermore, a non-targeting sgRNA (sgControl) obtained from the Human GeCKOv2 CRISPR knockout pooled library (88) was used as a negative control. Transcription is driven by RNA polymerase-III dependent U6 promoter, which requires a 5'-G at the transcription initiation site for efficient expression (89). Therefore, a G nucleotide was added at the 5' end of sgBeta and sgDelta making them 21 nt long (table 1). The DNA sequence for sgAlpha and sgGamma already started with a G nucleotide, therefore this was not necessary for these sgRNAs.

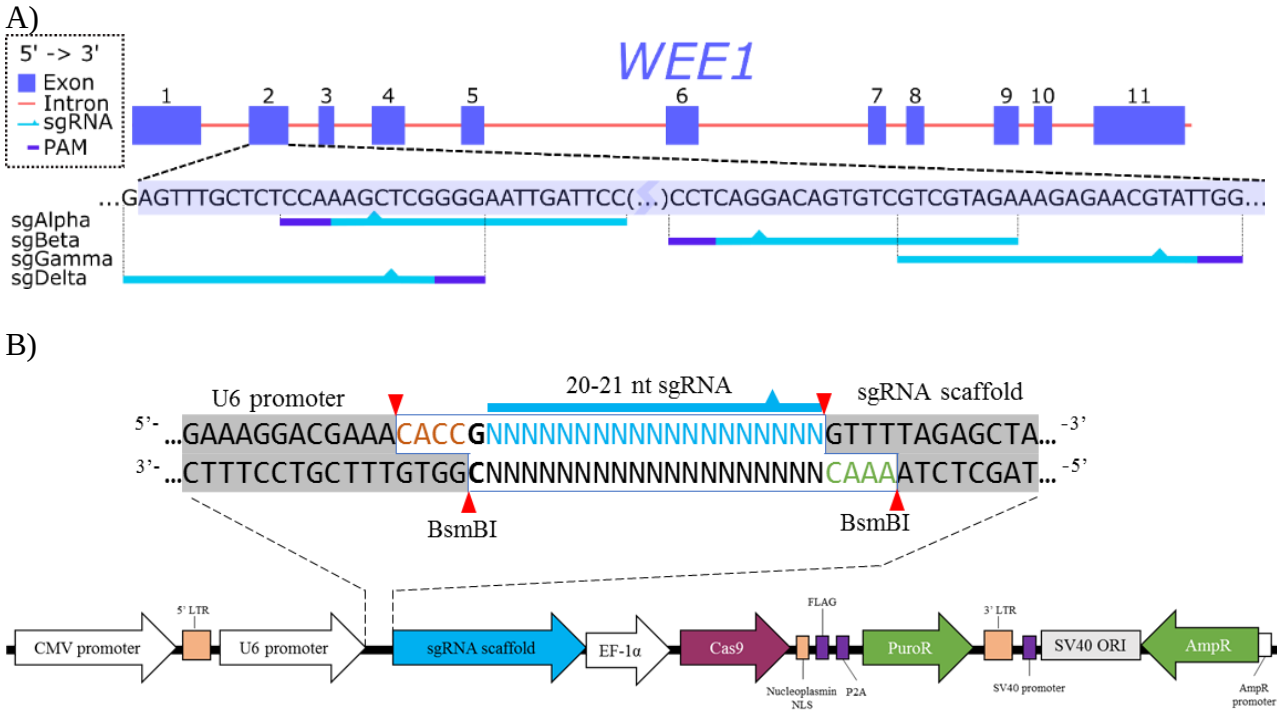

Figure 5) **Target sites for the four sgRNAs and cloning into plasmids**. (**A**) Exons and introns of *WEE1* are shown on top. A detailed depiction of exon 2 below shows the target for each sgRNA, their corresponding PAM sequence, and the expected Cas9 cleavage site. (**B**) sgRNAs targeting *WEE1* (blue text and line) were annealed to a complementary strand creating oligos with 5' overhangs (blue box). These were cloned into a plasmid vector backbone (grey boxes) by using the BsmBI restriction enzyme (cleavage sites are indicated with red arrows) as shown on top. An overview of the plasmid backbone and most important features is depicted on bottom, and the full plasmid construct can be found in supplementary figure 1.

Name	sgRNA sequence	PAM	Target start location / strand
sgAlpha	5' - GGAATCAATTCCCCGAGCTT - 3'	TGG	Chr11:9575920 / Negative
sgBeta	5' - **G**TCTACGACGACACTGTCCTG - 3'	AGG	Chr11:9576054 / Negative
sgGamma	5' - GTCGTAGAAAGAGAACGTAT - 3'	TGG	Chr11:9576066 / Positive
sgDelta	5' - **G**AGTTTGCTCTCCAAAGCTCG - 3'	GGG	Chr11:9575887 / Positive
sgControl	5' - ACGGAGGCTAAGCGTCGCAA - 3'	-	-

Table 1 **Information on the five sgRNAs of 20-21 nucleotides used and their target** sites. The added G nucleotides are underlined. PAM, Protospacer adjacent motif.

2.2 Cloning of sgRNA guides into plasmid vectors

2.2.1 Verification of plasmid

Prior to the initiation of cloning experiments, LentiCRISPR v2 plasmid (supplementary figure 1A) was verified using NheI (NEB, USA, Cat. No.: R0131S) and BamHI (NEB, Cat. No.: R0136S) restriction enzymes both alone and in combination and was digested at 37°C for 2 h. Gel electrophoresis at was conducted using 20 µL of the product and was mixed with loading dye (Thermo Scientific, Cat. No.: R0611). Agarose gels were made by dissolving agarose in 1X tris-acetate-EDTA buffer (TAE) buffer (Thermo Scientific, Cat. No.: B49) and subsequent heating. The intercalating agent, GelRed® Nucleic Acid Gel Stain (Biotium, Cat. No.: 41003), was then added. Here, samples were run along with negative plasmid controls on a 2% agarose gel placed in 1X tris-acetate-EDTA buffer (TAE) buffer (Thermo Scientific, Cat. No.: B49) at 100 V (supplementary figure 2).

2.2.2 Cloning

sgRNAs were ordered as complimentary oligonucleotides (oligos) with overhangs and 5' phosphorylation (TAGC, TAG Copenhagen). Annealing of 10 µM of sense and antisense oligos was performed using 1X DNA Ligase Buffer (Thermo Scientific, Cat. No.: B69) at 95°C for 5 min in a thermocycler (Techne, Prime thermal cycler) followed by cooling to room temperature (RT). The annealed oligos were subsequently cloned into the BsmBI-BsmBI site of the LentiCRISPR v2 plasmid backbone (figure 5B) (Addgene plasmid #52961 (88)). This was performed in a single-step digestion-ligation cloning reaction (table 2A) in a thermocycler (Biorad, T100™ Thermal Cycler) (table 2B).

A. Digestion-ligation reaction

Reagent	Volume	Final concentration
Fast digest buffer (Thermo Scientific, FD0454)	2 µL	1X
DL-Dithiothreitol (DTT, Sigma)	2 µL	1 mM
dATP (Thermo Scientific, Cat. No.: R0141)	2 µL	1 mM
LentiCRISPR v2	X µL	1.25 ng/µL
Annealed oligos	1 µL	2.5 nM
Fast Digest Esp3I (Thermo Scientific, Cat. No.: FD0454)	1 µL	0.5 U/µL
T7 ligase (NEB, Cat. No.: m0318L)	1 µL	150 U/µL
H_2O	To 20 µL	

B. Thermal cycler program

Step	Temp.	Time	Cycles
Digestion	37°C	5 min	6X
Ligation	22°C	5 min	

Table 2) **Setup for the 20 µL digestion-ligation reaction**. Esp3I is a BsmBI isoschizomer (**A**), and the thermal program used subsequently (**B**).

2.2.3 Transformation and bacterial amplification

Two µL of cloned plasmid DNA was transformed into One Shot™ Stbl3™ Chemically Competent E. coli (Invitrogen, Cat. No.: C737303) through Heat Shock in accordance with the manufacturer's instructions. Briefly, 2 µL of the digestion-ligation product was mixed gently with a vial of chemically competent One Shot Escherichia Coli (*E. Coli*) cells and incubated on ice for 30 min. The cells were then Heat-shocked by placing the vials in a water bath set to 42°C for 45 s. They were then incubated on ice for 2 min and 250 µL prewarmed S.O.C medium was added. The cells were incubated at 37°C on shaker set to 250 rpm for 1 h. Transformed E. Coli were cultured at 37°C overnight on LB-agar plates containing 100 µg/mL ampicillin (BioChemica, #A0839). Three individual positive colonies were picked from each plate, resuspended in 5 mL LB medium supplemented with ampicillin and incubated for 8 h at 37°C while shaking at 200-250 rpm. The bacterial liquid cultures were then diluted 1:500 in fresh LB medium and incubated for 16 hours (overnight) at 37°C while shaking at 200-250 rpm. Plasmid were purified using the GeneJET Plasmid Midiprep Kit (Thermo Scientific,

Cat.No.: #K0482) according to the manufacturer's instructions. Briefly, cells were harvested by centrifugation at 5,000 × g for 10 min at 4°C. Supernatant was discarded and the pellet was resuspended in a resuspension solution. This was followed by resuspension in Lysis Solution, Neutralization Solution Endotoxin Binding Reagent, and finally 96% ethanol in 50 µL centrifugation tubes. The tubes were centrifuged at 5,000 × g at RT and supernatant was subsequently transferred to new centrifugation tubes where 96% ethanol was added once again. The samples were then transferred to centrifugation tubes containing pre-assembled columns. Next a series of washing steps was initiated using Wash solution I and Wash solution II separated by centrifugation steps at 3,000 G for 2-5 min. Lastly, plasmids were eluted by using 350 µL elution buffer and concentrations were then measured by spectrophotometry (DeNovix DS-11). Purified plasmids from positive colonies were verified for insertion of sgRNAs by Sanger sequencing.

2.2.4 Polymerase chain reaction (PCR) and gel electrophoresis

Backbone-specific PCR primers flanking the restriction sites were designed for the verification of positive clones containing sgRNA inserts (*supplementary table 1*). The plasmids were used in a 25 µL PCR reaction containing 1 ng template, 1X Dreamtaq PCR Mastermix (Thermo Scientific, Cat. No.: K1081), and final concentrations of 0.2 µM forward and reverse primer. The thermal program for the PCR reaction was: 1 cycle at 95°C for 2 min, 35 cycles consisting of denaturation at 95°C for 30 s, annealing at 56°C for 30 s, and extension at 72°C for 1 min, and lastly 1 cycle of final extension at 72°C for 10 min. Subsequent to PCR, gel electrophoresis was conducted using 10 µL of the PCR amplicons mixed with loading dye (Thermo Scientific, Cat. No.: R0611). These were run along with negative controls on 1.5% agarose gels as described above. A 1kb ladder (Thermo Scientific, Cat. No.: Sm0311) or a 100bp ladder (Thermo Scientific, Cat. No.: Sm0321) was used to measure amplicon lengths.

2.3 Cell culture

Human embryonic kidney 293T cells (HEK293T) and the DLBCL cell line called OCI-Ly7 were used in this project. All cell cultures were maintained in cell culture flasks, 10 cm cell culture dishes, and cell culture plates at 37°C and a humidified atmosphere with 5% CO_2 in air. They were regularly passaged to maintain optimal density and to ensure access to fresh media.

The adherent HEK293T cells were cultured in growth medium consisting of Dulbecco's modified Eagle's medium (DMEM) (Gibco, ref: 31966-021 or ref: 21969-035) containing 10% Fetal Bovine Serum (FBS) (Gibco, ref: 10270-106) and 1% penicillin/streptomycin (P/S) (Life Technologies, Cat. No.: 15140122). Passaging was done by removing the old media containing debris and dead cells,

rinsing once with phosphate buffered saline (PBS) (Gibco, Cat. No.: 14200-067) and trypsinization with Trypsin-EDTA (Gibco, Cat. No.: 25300-054) at 37°C for 3-5 min. After the cells detached from the surface, trypsin was inactivated in prewarmed growth medium and the cells were centrifuged at 300g for 5 min at RT. They were then seeded in fresh, prewarmed growth medium.

OCI-Ly7 is a DLBCL cell line which grows in suspension as large clusters. These cells were cultured in Rosewell Park Memorial Institute (RPMI) Medium 1640 (Gibco, Ref: 52400-025) with 10% FBS and 1% P/S. Passaging was performed every 3-4 days at which cells were seeded at 0.5×10^6 cells/mL after centrifugation at 1200 RPM (240g) for 5 min at RT. The cells were at each passage counted with trypanblue (Life Technologies, Cat. No.: 15250061) to examine viability and adjust seeding density.

2.3.1 Transfection and puromycin selection of HEK293T cells

The cloned plasmids containing the sgRNAs of interest (pLv2-sgRNA) are denoted pLv2-sgAplha, pLv2-sgBeta, pLv2-sgGamma, pLv2-sgDelta, and pLv2-sgControl. Each plasmid was transfected into HEK293T cells using the Calcium Phosphate Transfection Kit (Invitrogen, Cat. No.: K278001). Briefly, 3×10^6 HEK293T cells were seeded in 10 cm cell culture dishes in 10 mL prewarmed growth medium. Next day, medium was changed an hour prior to transfection and only 9 mL was added. One mL transfection mixture consisting of 13 µg plasmid of interest, 50 µL 2M $CaCl_2$, and HEPES Buffered Saline (HBS) was incubated for 15 min at RT forming calcium phosphate precipitates. The precipitates were slowly dripped onto the cells and the dishes were placed in the cell culture CO_2 incubator. The medium was changed 24 h post transfection and cells left to recover for additional 24 h. Transfection was completed after 48 h, and the cells were subsequently used for further experiments.

To obtain a population of positively pLv-sgRNA transfected cells, puromycin selection was applied 48 h after transfection with the pLv-sgRNAs. Selection was performed by culturing the cells in growth media containing 0.5 µg/mL puromycin (Gibco, Cat.No.: A1113802) for 14 days alongside non-transfected HEK293T cells. Due to the puromycin resistance gene on these plasmids (supplementary figure 1A*)*, transfected cells survived the puromycin treatments. The media was changed every 2-3 days, and the cells were passaged to a different culture flask or plate in accordance with their confluency if needed.

Prior to transfection with the plasmid constructs containing the sgRNAs, transfection efficiency was tested and optimized using the lentiCRISPRv2GFP plasmid (Addgene plasmid #82416, (90)), which is a modified LentiCRISPR v2 vector in which the puromycin resistance gene has been replaced with

enhanced green fluorescent protein (eGFP) gene (supplementary figure 1B). Transfection efficiency was measured 48 h post transfection by flow cytometry (Cytoflex flow cytometer from Beckman Coulter, Life Science) where eGFP signal was detected on the fluorescein isothiocyanate (FITC) channel, and data was analyzed using the CytExpert software. Fluorescence images of the eGFP containing cells were taken using Zeiss Axio Observer Z.1 immediately prior to flow cytometry, and images were processed using the Fiji software (91).

2.4 Analysis of indel formation

2.4.1 Genomic DNA purification

Following selection of the positively transfected cells, genomic DNA (gDNA) was purified with the PureLink® Genomic DNA Kit (Invitrogen, K1820-01) from 2×10^6 cells or with DNeasy Blood & Tissue Kit (Qiagen, Cat. No.: 69506) in accordance with the manufacturer's protocols. DNA concentrations were measured by spectrophotometry.

2.4.2 PCR amplification, amplicon purification, and sanger sequencing

The purified gDNA was used as template in a PCR reaction using the Phusion Hot Start II DNA Polymerase kit (Thermo Scientific, Cat. No.: F549L). Through a series of optimizations, the PCR reaction in table 3A was used and the product was amplified using the thermal cycler program shown in table 3B. Gel electrophoresis on the amplicons was performed as described above, using 10 µL of the reactions mixed with loading dye in a 1.5% agarose gel. The rest of the PCR reaction was purified with GeneJET PCR Purification Kit (Thermo Scientific, Cat. No.: K0701) following the manufacturer's instructions. Briefly, purification of PCR reactions was initiated by adding a 1:1 volume of binding buffer to the PCR mixture. The solution was transferred to purification columns and centrifuged. The supernatant was then discarded, a Wash buffer to the columns which were centrifuged again. This step was repeated once more without the addition of Wash buffer to remove residual wash buffer. Lastly, columns were placed in clean microcentrifuge tubes and DNA was eluted using 25 µL elution buffer. All centrifugation steps were carried out at 12,000 g for 1 min at RT. The purified PCR amplicons were then Sanger sequenced (Eurofins Genomics, Tubeseq) with the same primers used in the PCR reaction.

A. PCR reaction

Reagent	Volume	Final concentration
GC buffer	10 µL	1X
dNTP mix (Themo Scientific, Cat. No.: R0191)	1 µL	200 µM each
Forward *WEE1* primer (10 µM)	0.5 µL	0.1 µM
Reverse *WEE1* primer (10 µM)	0.5 µL	0.1 µM
DMSO	1.5 µL	3%
Template (gDNA)	X µL	1 ng/µL
Phusion Hot Start II DNA Polymerase (2 U/µL)	0.5 µL	0.02 U/µL
H_2O	To 50 µL	

B. Thermal cycler program

Step	Temp.	Time	Cycles
Initial denaturation	98°C	30 s	1
Denaturation	98°C	10 s	25
Annealing	68°C	20 s	
Extension	72°C	30 s	
Final extension	72°C	10 min	1

Table 3) PCR reaction on genomic DNA using the Phusion Hot Start II DNA Polymerase kit performed in a 50 µL reaction (A), and the thermal program used subsequently (B).

3.4.3 Software analysis of indel formation

To evaluate the editing- and knockout efficiency of *WEE1* induced by each sgRNA, the Inference of CRISPR Edits (ICE) tool was used (Synthego, https://ice.synthego.com). Here, sequenced PCR amplicons from cells transfected with sgRNAs targeting *WEE1* were compared to amplicons from cells transfected with sgControl. These are used as input along with the sgRNA sequence. The software tool outputs an ICE score indicating the indel percentage, a KO-score corresponding to the percentage of indels that result in frameshift or are 21+ bp in length, as well as an assessment of how well the Sanger sequence data of the of the edited sample fits the proposed indel distribution. Output also includes visual representation useful for interpreting indels and quality checking.

2.5 Lentiviral production and transduction

Since B-cells are generally considered difficult to transfect with plasmid vectors and chemical based transfection methods can result in increased toxicity and cell death (81), 3rd generation lentiviral vectors targeting *WEE1* were produced in HEK293T cells in a laboratory suited for biosafety level II work. Lentiviral particles were produced through the calcium phosphate transfection as previously described with modifications described below.

Twenty-four hours after seeding, HEK293T cells were co-transfected with the lentiviral envelope and packaging plasmids (supplementary figure 1C-E): 3,75 µg pMD2.G (Addgene plasmid #12259), 3 µg pRSV-Rev (Addgene plasmid #12253), 13 µg pMDLg-pRRE (Addgene plasmid #12251), along with 13 µg of the transfer plasmids (pLv2-sgRNA or lentiCRISPRv2GFP). Media was changed 24h post transfection. Virus was harvested 48h and 72h post transfection by careful aspiration of the supernatant. Each harvest was centrifuged at 400 g for 5 min at RT to pellet packaging cells and cell debris. The supernatant was filtered through a 0.45 µm filter ensuring no cellular transfer, collected

in centrifuge tubes and stored at 4°C in between harvests. The harvests were pooled adding up to 40 mL of viral supernatant, aliquoted to cryotubes, and stored at -80°C.

2.5.1 HIV p24 ELISA assay

The concentration of the viral p24 capsid protein in the cell culture supernatant was measured to determine virus yield. This was achieved using the HIV-1 p24 ELISA Kit (Abcam, Cat. No.: ab218268) according to the manufacturer's instructions. Here, standard curve dilutions were prepared in concentrations ranging from 4.69 pg/mL to 300 pg/mL by using an included HIV-1 p24 Lyophilized Recombinant Protein and corresponding diluents. Samples consisted of already centrifuged and filtered viral supernatants. Using included 96-well strips, 50 µL of samples or standards were loaded into the wells in duplicates. A two-fold dilution of the lentiviral construct containing lentiCRISPRv2GFP was made using an included sample diluent and was loaded to a single well. In addition, 50 µL of an antibody cocktail (consisting of a capture antibody labelled with an affinity tag and detector antibody conjugated with a reporter) was added to the wells, in order to capture the analytes in solution and form a complex. The wells are precoated with anti-tag antibodies which immobilizes the entire complex through immunoaffinity. The strips were placed in a plate frame, and incubated on a plate shaker set to 400 rpm for 1 h at RT. The wells were washed three times in an included Wash Buffer, a TMP solution was added and the plate was incubated 10 min protected from light. A stop solution was then added and absorbance at 450 nm was determined using EnSpire Multimode Plate Reader (PerkinElmer). Concentrations of samples were determined using a standard curve generated from the standard dilutions with known concentrations. Data was analyzed in GraphPad Prism 6.

2.5.2 Lentiviral purification and transduction of OCI-Ly7 cells

Transduction efficiency of OCI-Ly7 cells was assessed twice using lentiviral particles containing the lentiCRISPRv2GFP transfer vector plasmid. In the first assay, the viral supernatant was used directly to transduce OCI-Ly7 cells. Here, 0.15×10^6, 0.3×10^6 and 0.4×10^6 OCI-Ly7 cells in growth medium were seeded in duplicates in 6-well plates. Volumes of 0.5 mL and 1 mL of the virus-containing supernatant equivalent to 12.2-49 pg p24 was added to the wells.

The rest of the viral supernatant was concentrated by ultracentrifugation using a Sorvall™ WX 90+ ultracentrifuge (Thermo, Cat. No.: 75000090) and polycarbonate bottles (Beckman, Cat. No.: 355654). First, 4 mL of 20% sucrose was added to the bottom of the ultracentrifuge bottles while samples were thawed to RT. The samples were then added to the bottles and ultracentrifugation through the sucrose cushion was performed at 25,000 g for 2 h at 4°C. The supernatant was removed,

and the virus-containing pellet was resuspended in PBS and pooled, resulting in a final volume of 200 µL virus.

In the second assay, the lentiviral constructs concentrated through ultracentrifugation was used for transduction. Here, 0.15×10^6 OCI-Ly7 cells were seeded in 6-well plates and all 200 µL of the concentrated virus equivalent to 0.83-1.67 ng p24 was added to a single well. The plates were incubated for 48 h. Fixation of the cells at was achieved by centrifugation at 300 g for 5 min at RT, followed washing in PBS, and resuspension in a 4% formaldehyde solution. After allowing the cells to be fixed for 10 min at RT they were washed once and resuspended in 500 µL in PBS. Flow cytometry and fluorescence imaging was performed to detect any eGFP containing cells.

Characterization and functional assays

The characterization and functional assays in this project were all conducted using HEK293T cells.

2.6 Cell counting

A simple cell counting assay was set up by plating four replicates of 0.4×10^6 transfected HEK293T cells in 6-well plates for 48 h and 72 h in growth medium. This was performed using NucleoCounter NC-200 (ChemoMetec, Allerod, Denmark) with Via1-Cassettes™ to determine live cell count and viability. Data was analyzed in GraphPad Prism 6.

2.7 Cell cycle analysis by flow cytometry

For cell cycle analysis, 1×10^6 cells were harvested by centrifugation at 400 g for 5 min at RT and resuspended in cold PBS. The cells were fixed in 70% ethanol for a minimum of 2 h. Preparation for flow cytometry was performed by spinning the cells down at 850 G and washing in 500 µL PBS twice. They cell pellets were treated and stained by the addition of a 250 µL mix of 100 µg/mL RNase A (Qiagen, Cat. No.: 19101) and 50 µg/mL propidium iodide (PI) (BioLegend, Cat. No.: 421301), before incubation at 37°C for 30 min protected from light. PI intensity was measured by flow cytometry (BD FACSCanto II from BD Biosciences) at a slow-medium flow rate of maximum 200 events/s. Data was processed using FlowJo software (v10.5.3) to determine cell populations in the G_0/G_1, S, and G_2/M cell cycle phases.

2.8 Vincristine dose-response screen

To investigate the effects of vincristine in *WEE1* knockout cells, a vincristine dose-response assay was conducted. The drug response assay was initiated by determination of the optimal vincristine concentration range that can be used in HEK293T. Cells were plated at a concentration of 0.03×10^6 cells per well in 120 µL growth medium in 96-well plates one day before all drug screens. First, a

series of two-fold dilutions from the stock concentration of vincristine (Oncovin, PharmaCodane, Aalborg Sygehusapotek) were prepared using saline as a diluent, and saline was used as a negative drug control. The cells were treated with 30 µL vincristine, equivalent to final concentrations ranging from 20 µg/mL to 0.00015 µg/mL per well for 48h.The same setup and vincristine concentration range was also applied on the *WEE1* knockout HEK 293T cells. Vincristine induced growth inhibition was assessed as the number of metabolically active cells by using the MTS-based assay, CellTiter 96® AQ_{ueous} One Solution Cell Proliferation Assay (Promega) according to the manufacturers protocol. Briefly, 30 µL of the CellTiter 96 Reagent (equivalent to 20% of the culture volume) was added to the wells and the plate was incubated for 2 h. Subsequently, absorbance was measured at 492 nm (FLUOstar Optima from BMG Labtech). To calculate the percentage of growth inhibition a plate with similar setup was measured at 0 h. First, absorbance in blank wells were subtracted from each well in both plates. Then, absorbance measured at 48 h was subtracted from 0 h. Growth inhibition is expressed relative to absorbance in control wells without drug addiction. Gaussian distribution was assessed using D'Agostino & Pearson omnibus normality test and two-way ANOVA was conducted using Dunnett's multiple comparisons test.

2.8.1 WEE1 inhibitor

A double drug assay using MK-1775 (Selleck Chemicals, Cat. No.: S1525), a WEE1 inhibitor, in combination with vincristine was conducted in wild-type HEK293T cells to compare the drug response in *WEE1* knockout cells to chemical WEE1 inhibition. MK-1775 stock was diluted in DMSO, which was also used in the negative drug controls. First, the optimal MK-1775 concentration range that can be used in HEK293T was determined by treating cells seeded as described above with increasing drug concentrations from 15.625 nM – 2,000 nM for 48 h and 72 h followed by an MTS-based analysis. A concentration of 125 nM MK-1775 proved to be the highest concentration which did not cause a growth inhibition and was thus chosen for the double drug assay (supplementary figure 3). Next, 125 nM MK-1775 was combined with eight vincristine concentrations ranging from 0.000610 µg/mL to 10 µg/mL. Cells were treated for 48 h with 125 nM MK-1775 combined with eight vincristine concentrations, vincristine only, and 125 nM MK-1775 only. Growth inhibition was measured by the number of metabolically active cells by the addition of CellTiter 96 Reagent (equivalent to 20% of the well volume) and MTS-based analysis was performed as previously described. All data from the drug screens was analyzed in GraphPad Prism 6.

2.9 Quantification of *WEE1* expression by droplet digital PCR

The expression of *WEE1* mRNA was quantified by droplet digital PCR using TaqMan Gene Expression Assay. This was performed in a stepwise manner as described below.

2.9.1 RNA purification and cDNA synthesis

For total RNA isolation, 5×10^6 cells were resuspended in 1 mL TRIsure™ (bioline, Cat. No.: BIO-38033) until the solution became homogenized. Samples were incubated at RT for at least 5 min and 0.2 mL chloroform was added to the samples followed by 10-15 s of vortexing. After another incubation at RT for 2 min, the tubes were spun down at 12,000 G at 4°C for 15 min allowing the mixture to separate into 3 phases. The upper RNA containing aqueous phase were transferred to a new Eppendorf tube. Final RNA isolation was performed in accordance with the mirVana™ miRNA Isolation Kit (Invitrogen, Cat. No. AM1561). Briefly, 1.25 volumes of 99.9% ethanol were added to the aqueous RNA containing tubes, and the mixture was passed through a filter cartridge by centrifugation at 10,000 G at RT for 15 s until the whole sample had passed through. The supernatant was discarded, and the filter was washed by adding 700 µL Wash solution 1 followed by centrifugation at 10,000g at RT for 5-10 s whereafter the flow-through was discarded. This was repeated twice with 500 µL of Wash Solution 2/3. The tubes were then centrifuged for an additional 1 min. The RNA was eluted with 50 µL preheated water in a new collection tube twice by centrifugation at maximum speed for 20-30 s. RNA integrity was evaluated using a Bioanalyzer (Agilent, 2100 Bioanalyzer) and concentrations were measured by spectrophotometry (NanoDrop™ 1000 Spectrophotometer).

The SuperScript™ III First-Strand Synthesis SuperMix Kit (Invitrogen, Cat. No. 11752-050) was used for first strand cDNA synthesis and was performed according to the manufacturer's instructions using 500 ng of RNA used as input to 20 µL reactions. The 2X reaction mix included in the kit is a cocktail that includes oligo$(dT)_{20}$, random hexamers, $MgCl_2$, and dNTPs required for the synthesis of cDNA and RNase inhibitors. This was mixed with an Enzyme Mix also included in the kit and 500 ng RNA. The samples were incubated in a thermal cycler at 25°C for 10 min, 50°C for 30 min, and lastly 85°C for 5 min. *E. coli* RNase H is also included and 1 µL (2U) was added to degrade RNA templates from cDNA:RNA hybrids after the reaction was complete. For each sample, a no-reverse transcriptase (NoRT) was included, using water instead of the RT Reaction Mix to check for genomic DNA contamination.

2.9.2 Droplet digital PCR

Droplet digital PCR (ddPCR) was prepared using 20X ddPCR™ Supermix for Probes (No dUTP) (Biorad, Cat. No.: 1863024) which is a ready-to-use mixture containing all components required for ddPCR, except primers, probes, and template. The polymerase included is inactive at ambient conditions but becomes activated during ddPCR due to its hot-start feature. Additionally, 2X TaqMan® Gene Expression Assay with probes labeled with 5' FAM™ reporter dye targeting either the target gene, *WEE1* (Applied Biosystems, Cat. No: 4351372) or the reference gene, TATA-box binding protein (*TBP*) (Applied Biosystems, Cat. No.: 4331182), were used (supplementary Table 1). This assay also includes primers targeting the genes of interest. A 17 µL master mix containing 1X of ddPCR Supermix and gene expression assays were mixed with 5 µL of RNA-equivalent cDNA (corresponding to 2 ng input). These were vortexed and incubated at RT for 3 min. To generate droplets, a DG8 cartridge (Bio-rad) was used in which 20 µL of the reaction was loaded to the sample wells and 70 µL Droplet Generation Oil (Bio-Rad) were loaded to the oil wells. The cartridge was placed and run on a QX200 Droplet Generator (Bio-Rad). Subsequently 40 µL of the generated droplets were transferred to a 96-well PCR plate and run on a thermal cycler with the program seen in table 4.

Step	Temp	Time	Cycles	Analysis Mode
Preincubation	95°C	10 min	1	None
Amplification	94°C	30 s	40	Quantification
	60°C	1 min		
Enzyme deactivation	98°C	10 min	1	None

Table 4) Thermal cycler program for ddPCR. A ramp rate of 2°C was used and samples were cooled down to 12°C after completion.

Fluorescent droplets were subsequently determined by counting PCR-positive and PCR-negative droplets using a QX200™ Droplet Reader and the coupled Quantasoft Software (Bio-rad). A minimum of 12,000 droplets were accepted for analysis of samples and results were expressed as copies/µL. To calculate all gene expression, the amount of RNA-equivalent cDNA added to each reaction was used to calculate the copies/ng for each sample. The expression of *WEE1* was divided by the expression of *TBP* to quantify relative expression of *WEE1* in all cell populations. Data was processed using GraphPad Prism 6.

3. Results

3.1 Annealing of oligos

sgRNAs targeting *WEE1* were designed and ordered as oligos with 5' overhangs to be cloned into the LentiCRISPR v2 plasmid. The overhang sequence for the sense strand was 5'-CACC, and 5'-AAAC for the antisense strand, making each oligo 24-25 bp long. To verify oligo annealing, the annealed oligos were loaded on a 2% agarose gel along with each single strand and gel electrophoresis was conducted (figure 6). The fluorescence signal from the binding of the intercalating GelRed agent were much stronger in wells loaded with the annealed, double stranded oligos (lane 3) compared to the bands from each single strand (lanes 1-2). As the annealed oligos are heavier due to being double stranded, the annealing could be confirmed by the shorter distance traveled through the gel in comparison to the single stranded samples.

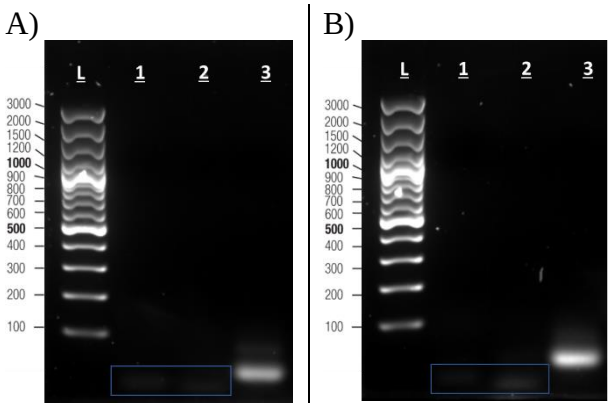

Figure 6) **Verification of oligo annealing by gel electrophoresis**. Here, sgAlpha (A) and sgBeta (B) are used as examples. Annealing of oligos was confirmed by the increased fluorescence intensity from binding of the GelRed and the shorter distance traveled through the agarose gels (lane 3 on both gels) in comparison to the single stranded oligos (blue boxes on lanes 1-2 on both gels) Samples were run through 2% agarose gels and a 100bp ladder was used as a reference for band size.

3.2 Cloning of the LentiCRISPR v2 plasmid

The LentiCRISPR v2 plasmid contains two restriction sites for BsmBI, resulting in the excision of an 1,885 bp fragment from the 14,873 bp large backbone after digestion (supplementary figure 1A). Gel electrophoresis with 18 µL of the product from a 20 µL digestion-ligation reaction using the BsmBI restriction enzyme, showed a faint band of the excised fragment (figure 7A) which could not be found in the negative plasmid control, undigested LentiCRISPR v2. The cloned plasmids (pLv2-sgRNA) were then transformed into *E.Coli*., purified from positively transformed cultures, and analyzed using PCR (figure 7B). The backbone specific primers used for the PCR reaction, target a region 247 bp upstream of the first restriction site for BsmBI (forward primer) to 212 bp downstream of the second restriction site (reverse primer) on the plasmids LentiCRISPR v2. The BsmBI restriction sites contains two different overhang sequences (5' CACC-3' and 5'-GTTT-3'), meaning that the plasmid

cannot self-anneal after digestion, but can only be annealed through ligation with the oligos containing the corresponding overhangs. Thus, a successful cloning reaction in which the 24-25 bp sgRNA-containing oligos are inserted, will produce an amplicon of 483-484 bp during PCR. In the case of unsuccessful cloning where the sgRNAs are not inserted, the amplicon length is 2,344 bp. Lanes 1-3 on figure 7B show the PCR results for pLv2-sgAplha after a positive digestion-ligation reaction and subsequent plasmid purification from three different *E. Coli* cultures, corresponding to successful cloning. On lanes 4-6, the negative PCR result from cloning of pLv2-sgBeta is shown, and the larger amplicons correspond to the negative plasmid control (PL), which was not cloned and therefore does not contain the inserts. Likewise, the rest of the sgRNAs were cloned into LentiCRISPR v2 in the same manner, over multiple attempts (supplementary figure 4).

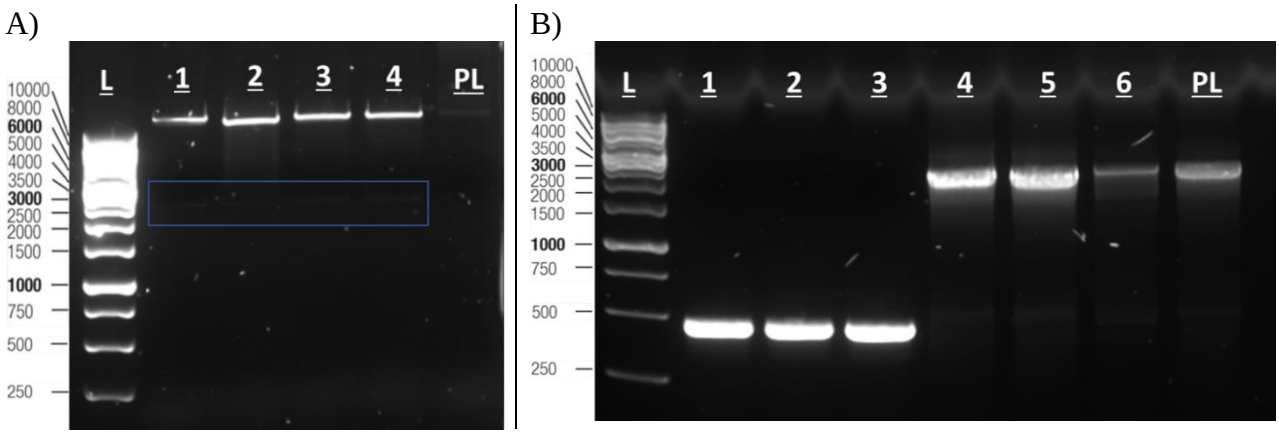

Figure 7) **Gel electrophoresis showing cloning results of pLv2-sgAlpha and pLv2-sgBeta.** (**A**) The digestion-ligation product from cloned plasmids pLv2-sgAplha (lane 1) and pLv2-sgBeta (lane 2) was loaded on a 0.8% agarose gel alongside minus-ligase controls (lane 3 and 4) and 50 ng undigested LentiCRISPR v2 plasmid (PL) which was not cloned. Blue square highlights the faint 1885 bp fragment cleaved out of the plasmid during digestion with BsmBI enzyme. Due to low visibility of this fragment, brightness was increased for visualization, consequently overexposing the ladder. (**B**) PCR products from pLv2-sgAplha (lane 1-3) and pLv2-sgBeta (lane 4-6) using primers flanking the sgRNA insertion site subsequent to plasmid purification from transformed E.Coli cultures. Samples were run through a 1.5% agarose gel. A 1kb ladder was used for both gels.

Subsequent to PCR and gel electrophoresis of all cloning reactions, each pLv2-sgRNA was Sanger sequenced to verify that all sgRNAs were correctly ligated using the same primers as the PCR reactions above detection. The chromatograms from the sequencing output was aligned with the sequences for each oligo using CLC Sequence Viewer 8 (QIAGEN bioinformatics). Figure 8 shows examples of sequencing chromatograms for pLv2-sgDelta, which is the plasmid construct containing sgDelta (figure 8A) and pLv2-sgControl, which is the plasmid construct containing the non-targeting sgControl (figure 8B). In addition, a complete alignment can be seen, where the sgRNAs can found in between each overhang. All cloning reactions were verified in the same manner through PCR followed by Sanger sequencing and alignment with oligo DNA sequences. For pLv2-sgAlpha, -Beta,

and -Gamma, the sequencing chromatograms showed mixed signaling with overlapping waves, however all oligos could still be detected manually (data not shown).

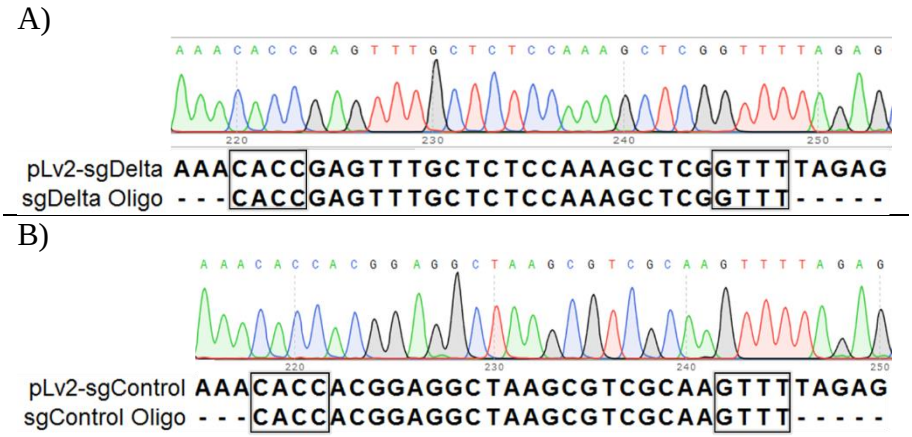

Figure 8) **Verification of positive PCR results from cloned pLv2-sgRNA by Sanger sequencing.** Example include pLv2-sgDelta (A) and pLv2-sgControl (B). In both cases clean traces in the sequencing chromatograms was seen. Complete alignment with oligos containing sgRNA sequences in between both overhangs (marked squares) confirmed that cloning was successful.

3.3 Transfection of HEK293T cells

To express the cloned plasmid constructs, HEK293T cells need to be transfected. Transfection efficiency of HEK293T cells was tested using lentiCRISPRv2GFP, which contains the cDNA sequence for a FLAG-tagged Cas9 protein followed by the P2A self-cleaving site and the sequence for the eGFP marker protein (supplementary figure 1B). Hereby, Cas9 and eGFP are produced as a single mRNA sequence which is cleaved during translation, indicating that eGFP producing cells co-express Cas9. HEK293T cells were transfected in duplicates using the calcium phosphate transfection method and flow cytometry analysis revealed a transfection efficiency of 97% and 99.3% 48 h post-transfection when compared to wildtype HEK293T cells (figure 9A). However, although many fluorescent cells could be detected by flow cytometry, prior fluorescence microscopy did not indicate such a high transfection efficiency as the cells were 80-90% confluent 48h post-transfection (figure 9B).

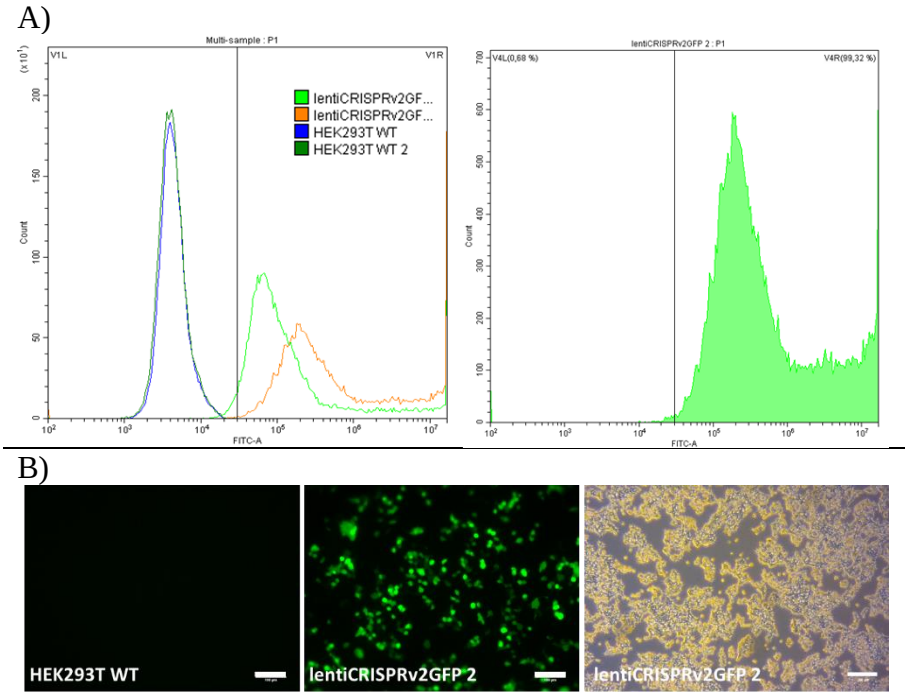

Figure 9) **Transfection efficiency of HEK293T cells 48 h post transfection with lentiCRISPRv2GFP.** (**A**) Flow cytometry analysis was conducted using CytExpert software. Subsequent to exclusion of cell debris from dead cells through gating, a vertical border was set above the maximum intensity on the FITC channel for the two HEK293T WT samples, to separate eGFP cells from background signal (left). The example (right) shows eGFP positive cells from one replicate. (**B**) Immunofluorescence analysis of eGFP expression on HEK293T WT (Left) and the same HEK293T transfected cells from above (middle), and a phase contrast image from the transfected cells for comparison. Scale bars: 100 µm

3.4 Lentiviral production

Based on the results from the transfection of HEK293T cells, the same protocol was used for lentiviral production. Here, HEK293T cells were co-transfection with pLv2-sgRNA alongside lentiviral envelope- and packaging plasmids. A lentiviral construct containing the lentiCRISPRv2GFP plasmid was also included (Lv2-GFP). Fluorescence microscopy of the Lv2-GFP producing cells showed the presence of fluorescent cells as previously observed, indicating successful transfection of the transfer plasmids (figure 10).

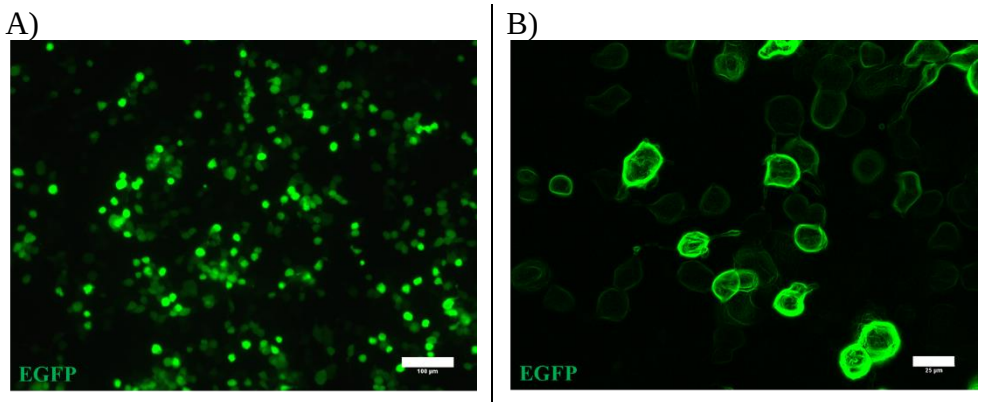

Figure 10) **Lentivirus producing HEK293T cells 72h post co-transfection with transfer-, envelope-, and packaging plasmids.** Scalebars: 100 µm (A) and 25 µm (B).

The concentration of the viral supernatants collected from the lentivirus producing cells was determined by HIV-1 p24 ELISA (figure 11). Despite using the same setup to produce all Lv2-sgRNAs, a large variation between each construct was observed, however within each duplicate, sample variation was ≤ 2.3 pg/mL p24. The concentrations of Lv2-sgGamma and Lv2-sgControl were below the minimum concentration used in the standard dilutions, which ranged from 4.69 pg/mL to 300 pg/mL p24, suggesting that barely any virus was produced. The highest concentration among the lentiviral construct was in Lv2-sgDelta at 45.7 pg/mL. A single sample consisting of a two-fold dilution of Lv2-GFP was also included in the assay (Lv2-GFP 50%). The concentration of this sample was expected to be 50% of the non-diluted sample (Lv2-GFP), however the concentration was approximately the same as before dilution.

A)

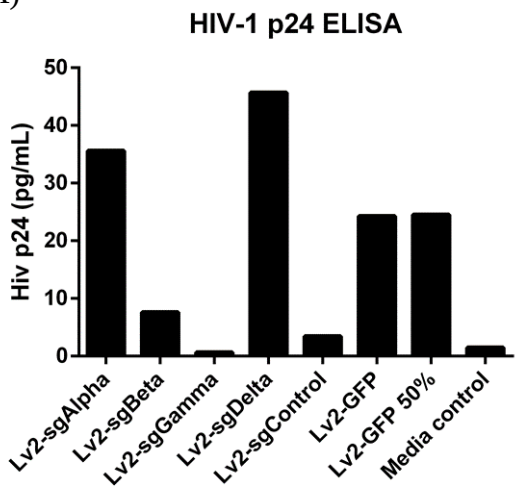

B)

Sample	**HIV_p24 (pg/mL)**
Lv2-sgAlpha	35.62
Lv2-sgBeta	7.62
Lv2-sgGamma	0.67
Lv2-sgDelta	45.70
Lv2-sgControl	3.42
Lv2-GFP	24.29
Lv2-GFP 50%	24.50
Media control	1.47

Figure 11) **Concentrations of lentiviral p24 proteins in the virus-containing supernatants** measured by ELISA (A). Concentrations were determined using standard dilutions and are shown in the table (B).

3.5 Transduction of OCI-Ly7 cells with the lentiviral constructs

Despite the difference in Lv2-GFP concentrations measured in ELISA, the viral construct was used to transduce OCI-Ly7 cells. First, the cells were transduced using 0.5 – 1 mL of the virus-containing supernatant, equivalent to 12.2-49 pg p24. eGFP signal could not be detected by flow cytometry nor by fluorescence microscopy, signifying that the concentrations used were too low (supplementary figure 5A). The rest of Lv2-GFPs were concentrated by ultracentrifugation and transduced to a single well containing 0.15×10^6 OCI-Ly7 cells. Despite a higher concentration used this time, transduction with the 0.83-1.67 ng p24 could barely be detected by flow cytometry (supplementary figure 5B) and fluorescent cells could not be detected by microscopy (data not shown).

Due to the low lentiviral p24 concentrations measured by ELISA, and the low transduction efficiency of OCI-Ly7 cells observed by flow cytometry and fluorescence microscopy when using the lentiviral eGFP constructs, we decided to continue the *WEE1* knockout experiments in HEK293T cells using the cloned pLv2-sgRNA plasmids and calcium phosphate transfection.

3.6 In vitro validation of *WEE1* knockout

To validate the efficiency of the sgRNAs, HEK293T cells were transfected using the optimized transfection approach as previously described. Transfections with pLv2-sgRNAs to knockout *WEE1* was performed over two times. First, sgAlpha and sgBeta samples were transfected and cultured alongside non-transfected HEK293T control cells. In the second transfection, sgGamma, sgDelta, and sgControl were used.

3.6.1 PCR on genomic DNA

Selection of transfected HEK293T cells was performed by puromycin treatment, gDNA was subsequently purified, and PCR was conducted using primers flanking all four sgRNA cut sites in *WEE1*. The amplicons produced through PCR on gDNA are 893 bp long and bands of the same length was observed by gel electrophoresis using the PCR product (figure 12A and 12B). An additional PCR reaction with the plasmid primers previously used to verify cloning was conducted on DNA isolated from sgGamma transfected HEK293T cells, and this showed that the plasmids were still present after puromycin selection (figure 12B, lane PL).

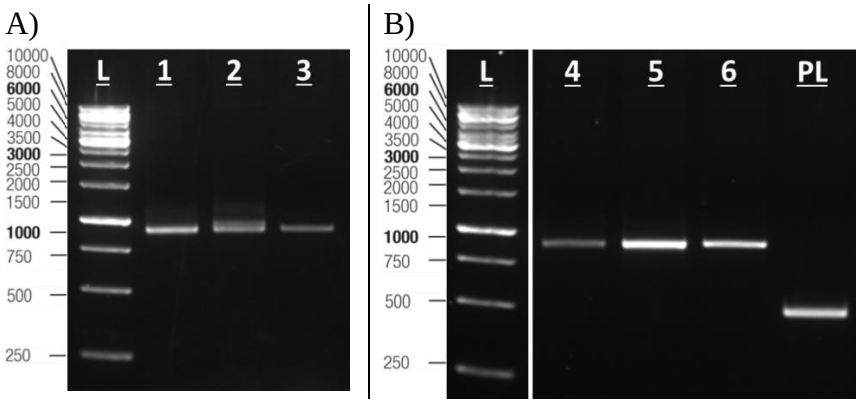

Figure 12) **PCR on genomic DNA from transfected and subsequently puromycin selected cells or controls.** Single bands corresponding to the expected amplicon lengths was seen in the gels from both the first transfection **(A)** (lane 1: sgAlpha, lane 2: sgBeta, lane 3: HEK293T WT), and from the second transfection **(B)** (lane 4: sgGamma, lane 5: sgDelta, lane 6: sgControl). In addition, by using primers targeting the transfected plasmids used for transfection on gDNA isolated from sgGamma samples, it could be observed that plasmids were still present after puromycin selection (B, lane PL).

HEK293T WT cells were used as controls for puromycin selection and were treated alongside the transfected cell populations. Puromycin selection of positively transfected cells was considered complete, once the control cells were all killed as they should not contain the puromycin resistance

gene. However, not all HEK293T control cells were killed during the puromycin selection of the cells from the second transfection. Therefore, the presence of plasmids was investigated in the surviving HEK293T control cells along with the transfected cell populations after puromycin treatment. Cloned plasmids were found at lower concentrations in the non-transfected HEK293T WT cell culture used as controls for puromycin selection, indicating contamination with plasmid containing cells (supplementary figure 3).

3.6.2 Analysis of indel formation

All PCR amplicons containing the sgRNA cut sites were Sanger sequenced and analyzed for indel formation using the ICE tool. As expected, no difference was observed between the sequencing chromatograms of cells transfected with sgControl and HEK293T WT. A complete alignment of this sequencing data indicated that no indels were formed in sgControl transfected cells (supplementary figure 7). DNA sequencing chromatograms for sgAlpha, sgBeta, sgGamma, and sgDelta were therefore compared to the sgControl in the ICE analysis. Analysis of the sequencing chromatograms from cells transfected with the *WEE1*-targeting sgRNAs showed multiple sequencing signals with low strength from the region surrounding the spCas9 cut sites and downstream. This indicates that spCas9 induced DSB formation, and subsequent reparation through the NHEJ pathway introduced various kinds of indel mutations in the process, making the transfected cells heterogenous (figure 13A). Further analysis of these chromatograms showed that the most predominant sequence present in the heterogenous cell population was still the WT sequence for sgAlpha (31.7%), sgBeta (25.3%), and sgGamma (38.6%) samples, whereas an +1 insertion was the most predominant sequence for sgDelta (16.8%) sample. The inferred sequences of the four edited populations were all different but consisted mainly of deletions (figure 13A).

The editing efficiency for all sgRNAs is presented as an ICE score (i.e. the percentage of non-WT sequence in the pool) and was generated by comparing the edited DNA sequence traces to the trace for sgControl. ICE scores were over 50% for all samples (sgAlpha: 61%, sgBeta: 68%, sgGamma: 58%, and sgDelta: 79%). The knockout score (KO) indicates the percentage of indels that leads to frameshift mutations, assuming all edits are within a coding region. The ICE tool revealed KO-scores of sgAlpha: 40%, sgBeta: 42%, sgGamma: 25%, and sgDelta: 43%, thereby correlating with the ICE scores for each sample (figure 13B).

Instead of using the PCR products directly for purification, gels were also loaded for sgAlpha and sgBeta PCR products in a previous assay. Subsequent to gel electrophoresis, bands corresponding to

the correct amplicon size were cut out from gels, purified, and Sanger sequenced. ICE analysis of these amplicons showed slightly higher Indel formations for sgAlpha (ICE: 74%, KO-score: 47%) and sgBeta (ICE: 70%, KO-score: 45%) when purifying from gels (supplementary figure 8). The DNA sequence traces the same for these samples compared to the once from above, with the main difference being, that they contained less WT-sequences (20% and 24.6% respectively) which suggests that there can be slight variations in ICE and KO-scores depending on purification method. However, a substantial DNA loss was observed when purifying from gels which prevented Sanger sequencing for some samples as concentrations were too low. All PCR products used for the analysis of indel formation were therefore purified directly for optimal comparison of editing efficiencies between all samples.

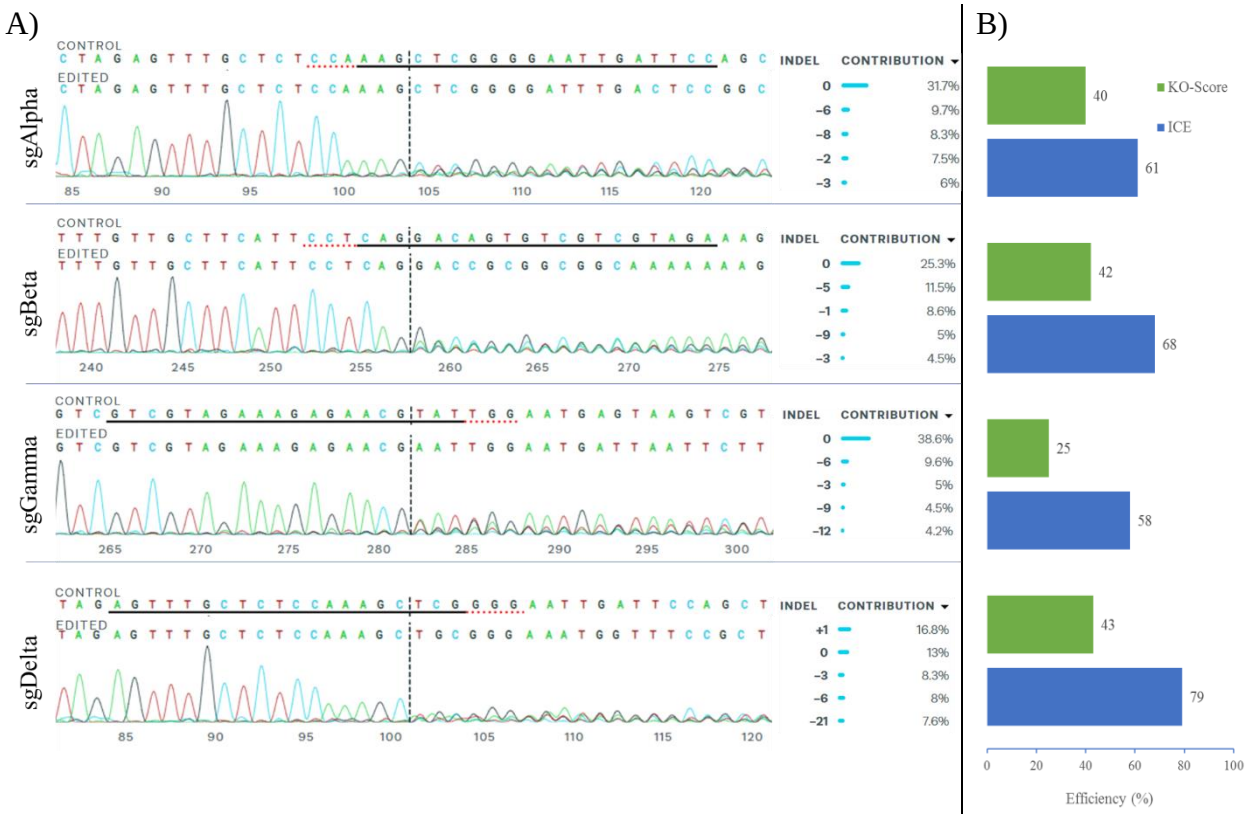

Figure 13) **Indel analysis of sgRNAs targeting *WEE1***. The ICE tool was used to analyze the indel formation of cells transfected with pLv2-sgRNAs. Subsequent to puromycin selection, a region surrounding the CRISPR/Cas9 target sites in *WEE1* was PCR amplified, amplicons purified directly, and Sanger sequenced. (**A**) Sequencing chromatograms displayed mixed signals with low amplitudes in the region surrounding the Cas9 cut site and downstream indicating that various indel mutations was formed, thus making the cell populations highly heterogenous. DNA bases shown on top are from the control with illustrated sgRNA sequences (black lines) and PAM site (red dots) and below are DNA bases from the most prominent peaks on chromatograms from edited samples. Examination of the top 5 indels revealed that mutations mainly consisted of deletions. (**B**) Quantification of sequencing chromatograms using the ICE tool showed high Indel percentages of 58-79%, and knockout scores of 25-43%, with sgDelta displaying the highest editing efficiency as is also indicated by the low amplitudes subsequent to the cut site.

The transfection of cells was split into two stages, and the following functional and characterization assays were conducted accordingly, necessitating careful comparison between both.

3.7 Cell growth after transfection with sgRNA containing plasmids

During cell culture, a difference in the growth rate was observed between HEK293T WT and cells transfected with sgAlpha and sgBeta plasmids subsequent to transfection and puromycin selection. Therefore, a cell counting assay was setup, in which 400,000 cells were seeded and counted after 48h and 72h. A slight difference in cell number could be observed after 48h, however the higher growth rate was more pronounced after 72h with 50% more HEK293T WT cells than the sgAlpha population and 68.4% more HEK293T WT cells than the sgBeta population (figure 14, left). The higher cell number was also observed, when comparing the same non-transfected cells with the sgGamma (30.7%), sgDelta (16.1%), and sgControl (21.4%) populations from the second transfection after 72 h, but not after 48 h. However, the slower growth rate observed after 72 h in the sgRNA transfected cells is likely not due to knockout of *WEE1*, but possibly due to the puromycin selection , as slightly less cells were counted in the sgControl population (which did not cause indels mutations in *WEE1*) compared to sgDelta (4.4% less). In addition, the sgControl population only had 7.6% more cells in comparison to the sgGamma population after 72 h (figure 14, right).

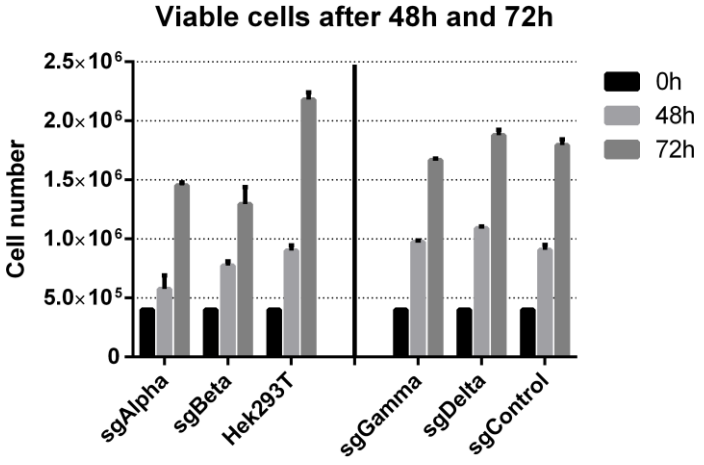

Figure 14) **Cell counting of sgRNA transfected cells in comparison to non-transfected control (n=4).** HEK293T WT cells exhibited a higher growth rate than sgRNA-transfected from both the first transfection (Left side) and the second transfection (Right side) after 72h, but not after 48 h. No substantial difference in growth rate was observed between the samples from the second transfection after 72h. The results are presented as mean ± SEM.

3.8 Cell cycle analysis

Due to the vital role *WEE1* plays in the G2/M phase transition, cell cycle analysis of the transfected cell populations was conducted. The cells were fixed in ethanol and stained with propidium iodide prior to flow cytometry. Prior to cell cycle analysis, all replicates (N=4) were manually gated and subsequently pooled (gating strategy shown on supplementary figure 9). In the heterogenous cell populations from the first transfection (sgAlpha and sgBeta) fewer cells could be observed in the

G2/M phase (10.4% and 11.5% respectively) than the HEK293T WT cells (17%). Additionally, a slight accumulation of cells was seen in the G1 phase (68.5% and 62%) and sub-G1 (7.24% and 10.7%) whereas for HEK293T cells only 55.7% were in the G1 phase and 4.61% sub-G1. In the cell populations from the second transfection, almost no differences were seen between sgGamma, sgDelta, and sgControl (figure 15).

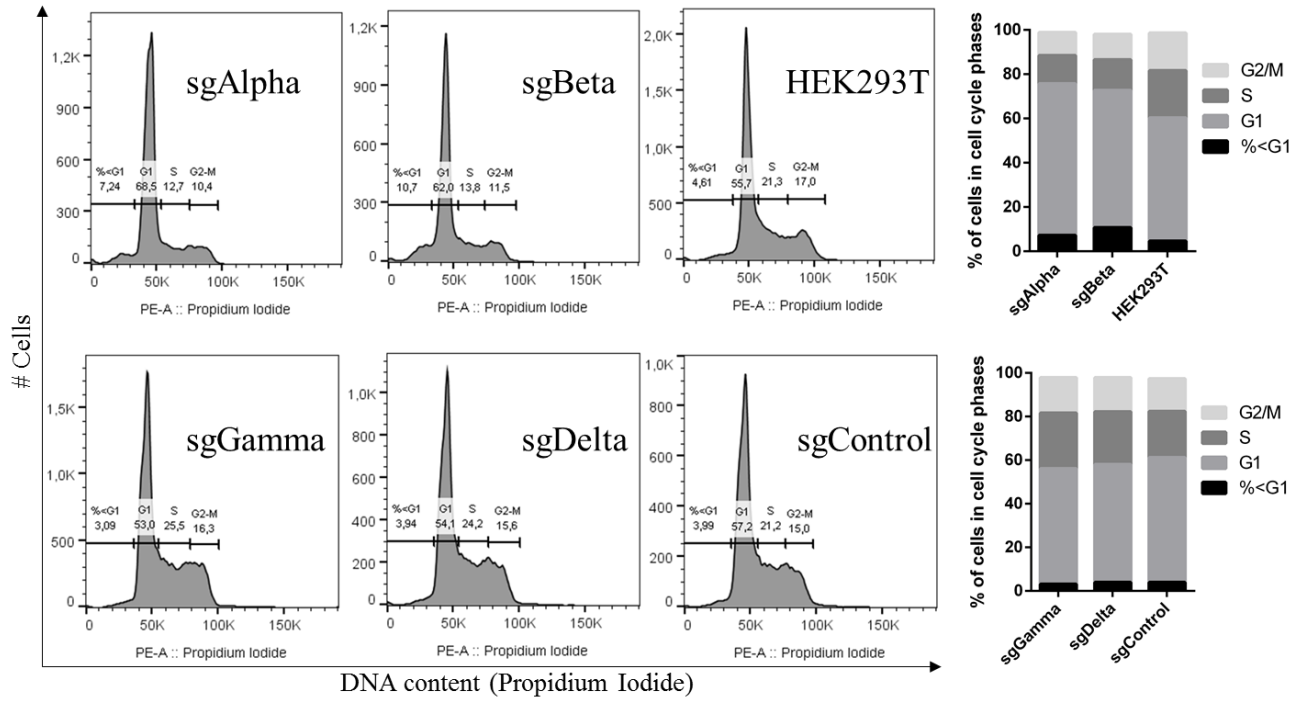

Figure 15) **Cell cycle analysis using propidium iodide.** Total amount of cells analyzed ranged from 13,334-21,916 after gating and pooling. Data from the first transfection is presented at the top, and data from the second transfection is presented below. Stacked bars to the right show the comparison between each cell cycle phase and cell population.

3.9 Droplet digital PCR

WEE1 mRNA expression was quantified using droplet digital PCR. mRNA expression of *TBP* was used as a reference. Expressions were measured as copies/ng from a PCR reaction using 2 ng RNA-equivalent cDNA as input and presented as relative gene expression of *WEE1* (figure 16). Subsequent to transfection with the *WEE1* targeting sgRNAs followed by puromycin selection, higher Wee1 mRNA expression was seen in the heterogenous cell populations compared to both the sgControl population and HEK293T. Almost no difference in the relative gene expression was seen between the controls. The highest expression was seen in the sgGamma population, in which *WEE1* expression was approximately twice as high as the controls. Interestingly, the expression of both the gene of interest (*WEE1*) and the reference gene (*TBP*) was much lower in cells from the first transfection (*WEE1*: 115.1-350.2 copies/ng; *TBP*: 48.3-87.9 copies/ng) than in the cells from second transfection

(*WEE1*: 259.9-535.2 copies/ng; *TBP*: 103.1-118.8 copies/ng). However, this difference does not play an important role in the final results, since they are presented as relative expression between both genes.

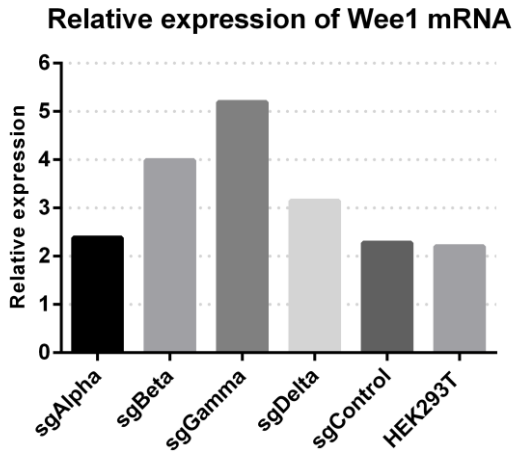

Figure 16) Relative expression of *WEE1* mRNA. ddPCR was conducted on transfected cells and HEK293T WT cells using 2 ng RNA-equivalent cDNA as input. mRNA expression of *WEE1* and the reference gene, *TBP*, was calculated to copies/ng and finally presented as the relative expression between *WEE1* and *TBP*.

3.10 Vincristine drug response assay

To investigate the effect of vincristine on *WEE1*-knockout cells, the heterogenous mix of cells was used in a drug response assay conducted separately on cells from each set of transfections. Vincristine induced growth inhibition was assessed relative to untreated controls and measured by number of metabolically active cells. First, a test run conducted on HEK293T WT cells using vincristine concentrations at 0.00015µg/mL - 20 µg/mL showed that GI50 (50% growth inhibition) was achieved at concentration 0.0391 µg/mL and 0.0781 µg/mL, well within the range. At the highest concentration (above 2.5 µg/mL) the maximal growth inhibition achieved was 14.5% to 18% metabolically active cells (supplementary figure 10).

The same vincristine concentrations were used on cells from both transfections. The non-transfected HEK293T cells used as controls in the first transfection showed a similar dose-response curve (GI50 at 0.0195 µg/mL-0.0391 µg/mL) (figure 17A). These cells were cultured alongside the transfected cells but was not treated with puromycin. sgAlpha and sgBeta cell populations displayed a significantly reduced growth inhibition ($P<0.0001$) at concentrations from 0.195 µg/mL when compared to the non-transfected controls (figure 17A). However, as the sgRNA transfected cell populations were selected by puromycin treatment prior to vincristine treatment, this difference

growth inhibition might not be due to knockout of *WEE1*, but could also indicate, that surviving cells become more resistant to vincristine after puromycin treatment.

The second transfection consisted of sgGamma, sgDelta, and sgControl cell populations that were all cultured alongside each other and treated with the same concentrations of puromycin (figure 17B). A significant growth inhibition could be observed in the sgDelta population when compared to the sgControl population at vincristine concentrations from 0.0391 µg/mL (P<0.0001). At the lower concentrations, a tendency towards growth stimulation was observed in the sgGamma population. However, a non-significant tendency towards increased growth inhibition was seen at concentrations higher than 0.156 µg/mL when compared to the sgControl population.

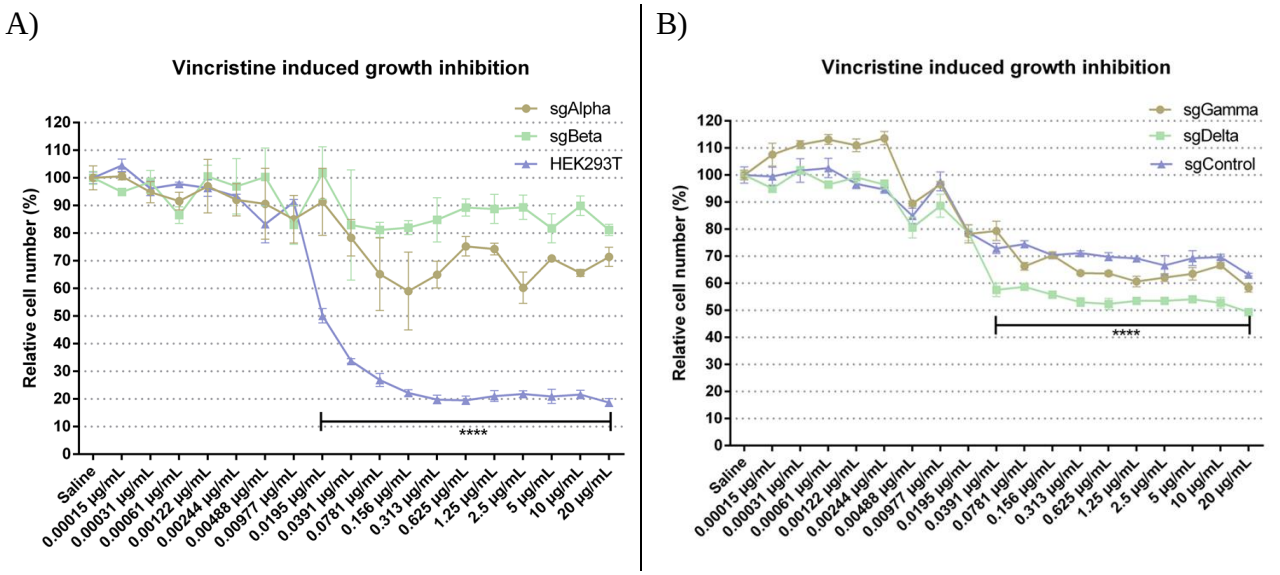

Figure 17) **Vincristine dose-response analysis measuring induced growth inhibition relative to untreated controls after 48 h.** HEK293T cells were transfected with two sgRNAs to knockout *WEE1* alongside the non-targeting sgControl, and HEK293T WT cells were used as non-transfected controls. The heterogenous mix of *WEE1* knockout cells were treated with either saline or increasing doses of vincristine (0.00015-20 µg/mL) for 48h. Number of metabolically active cells (n=3) were measured using 3-(4,5 dimethylthiazol-2-yl)-5-(3-carboxymethoxyphenyl-2-(4-sulfophenyl)-2H-tetrazolium assay. Drug response is shown as percentage of living cells relative to the no-drug condition. (A) A significantly decreased growth inhibition was observed in the puromycin selected sgAlpha and sgBeta cell populations when compared to HEK293T WT cells (****p<0.0001). (B) The sgDelta cell population displayed signinificant growth inhibition at high vincristine concentrations when compared to sgControl, whereas the sgGamma population only displayed a non-significant tendency towards the same response. Gaussian distribution was assessed using D'Agostino & Pearson omnibus normality test and two-way ANOVA was conducted using Dunnett's multiple comparisons test where a value of P<0.05 was considered statistically significant. Results are presented as mean ± SEM.

3.10.1 WEE1 inhibition

To compare the vincristine response in the heterogenous *WEE1* knockout cells to chemical inhibition of WEE1, A double drug assay was conducted on HEK293T WT cells using the WEE1 inhibitor, MK-1775, in combination with vincristine. As previously mentioned, a concentration of 125 nM MK-1775 was chosen, based on an assay using 15.625 nM – 2,000 nM MK on HEK293T WT cells. This was the highest concentration used, which did not cause growth inhibition by itself after 48 h as

measured by MTS assay (99.2% metabolically active cells) (supplementary figure 3). In addition, at concentrations higher than this, rounding of cells and increased number of dead cells could be seen using phase contrast microscopy. These characteristics were also observed to a higher degree when treated the cells with the highest concentrations of vincristine and MK-1775 (data not shown).

In the double drug assay, the effect 125 nM MK-1775 in combination with increasing vincristine concentrations was testes on HEK293T WT cells, using vincristine only, MK-1775 only, and untreated cells as controls. As expected, none of the treatment controls displayed growth inhibition. A tendency towards increased growth stimulation was observed at lower vincristine concentrations for both the double drug assay and the vincristine only samples. As can be seen on figure 18, 125 nM MK-1775 did not cause a significant difference in growth inhibition after vincristine treatment since the dose-response were the same for cells treated with vincristine only. Interestingly, the HEK293T cells treated only with vincristine exhibited less growth inhibition in this assay compared to the vincristine assays conducted previously.

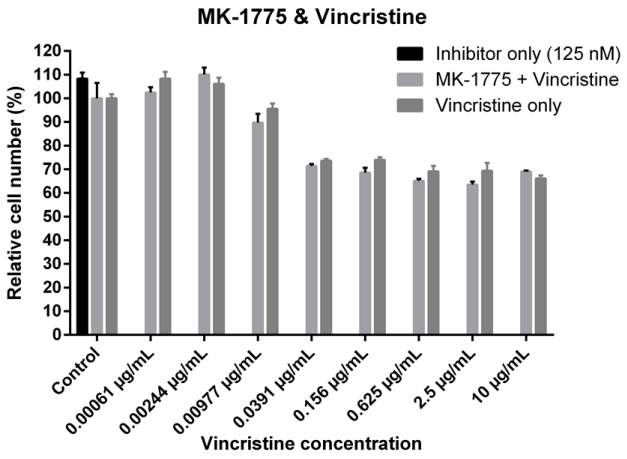

Figure 18) **Chemical inhibition of WEE1**. HEK293T cells were either treated with a combination of MK-1775 and vincristine or vincristine only. MK-1775 was dissolved in DMSO and vincristine was dissolved in saline. For the double drug assay, the non-treatment control consisted of HEK293T cells with 30 µL DMSO, and an inhibitor only control was used here. For the treatment control of vincristine only wells, 30 µL saline was added. Number of metabolically active cells (n=3) were measured using 3-(4,5 dimethylthiazol-2-yl)-5-(3-carboxymethoxyphenyl-2-(4-sulfophenyl)-2H-tetrazolium assay. Drug response is shown as percentage of living cells relative to the no-drug condition. Results are presented as mean ± SEM

4. Discussion

In this study, the role of *WEE1* in the response to vincristine was investigated. This was pursued by first designing four sgRNAs targeting exon 2 in *WEE1* in order to induce a CRISPR/Cas9 mediated gene knockout. All sgRNAs were successfully cloned into lentiviral transfer plasmids which were transfected into HEK293T cells and used to produce lentiviral vectors suitable for transduction of DLBCL cells. Cells were transfected and gene editing efficiencies for each sgRNA were investigated using the ICE tool. Lastly characterization and functional assays were conducted.

4.1 Production of lentiviral vectors to transduce OCI-Ly7 cells

As the overall aim of this study was to investigate the role of *WEE1* in the response to vincristine in DLBCL, the vincristine resistant OCI-Ly7 cell line was chosen for the vincristine drug response assays. To transduce the OCI-Ly7 cells, the quantities of lentiviral particles harvested from HEK293T packaging cells were measured. The viral titers measured by ELISA proved to be too low for eGFP detection in transduced cells when using flow cytometry and fluorescence microscopy. The highest quantities used for transduction was 0.83-1.67 ng p24 to 0.15×10^6 OCI-Ly7 cells. In a previous study, a much higher quantity of 80 ng p24 was proven effective in inducing knockout of target genes in OCI-Ly7 cells by using the same setup and approach as this study (85). By using a modified LentiCRISPR v2 plasmid along with the same lentiviral envelope and packaging plasmids as used in this study, lentiviral vectors targeting the murine Vegfa gene have previously been produced (92). A quantity of 500 ng p24 to 0.2×10^6 HEK293-VEGFA cells showed high transduction efficiency in four of five transductions when measured by immunofluorescence analysis of eGFP signal (92). Generally, higher p24 quantities are used when transducing in vitro cell lines efficiently than the quantities used this study (93–95). Taken together, this indicates that the lentiviral constructs were produced with very low titers and p24 yields in this study, explaining why we did not observe a fluorescent signal.

p24 ELISA measures the total amount of p24 capsid protein in the sample regardless of whether it is incorporated into a viral particle, determining the physical viral titer based on this might lead to an overestimation of the functional vector titer, as free p24 and non-functional vectors are also measured (83). Another drawback for this titration method include a generally high variation in p24 concentrations measured by ELISA and the extensive dilutions often performed prior to titration, both of which affects the reproducibility of the results (83).

Despite being a fast and method for controlling whether any lentivirus has been produced, determination of physical p24 titer does not provide information about functional vector titer needed to transfect the cells (83). A determination of the multiplicity of infection (MOI), which is the number of infectious particles per cell by using fluorescence microscopy and flow cytometry, is thus more useful to assess the infectivity of the produced lentiviral particles (96). However, as the entire undiluted lentiviral stock was used for transduction to one well, and flow cytometry could still not reliably determine the functional titer (the number of transduced cells), the optimal lentiviral concentration that results in eGFP producing OCI-Ly7 cells remains unknown. Hereby the lentiviral concentration needed to transduce OCI-Ly7 cells also remains unknown. The reason for the low lentiviral titers is likely not due to a low transfection efficiency in HEK293T cells during lentiviral production, since fluorescence microscopy showed a high transfection efficiency 72 h post-transfection of the lentivirus producing packaging cells (figure 10). In addition to the transfer vector, the cells were also co-transfected with lentiviral envelope and packaging plasmids. Perhaps the quality or quantity of these plasmids were too low, since it has previously been shown that manipulation of the amounts of plasmids used for lentiviral production can influence concentration (pg p24/mL) of lentiviral vectors in supernatant (97). In addition, the infectivity of lentiviral particles in supernatants can also be increased by harvest from serum-free medium, and this might have impacted the ineffective transduction of OCI-Ly7 cells in this study (97).

4.2 Using HEK293T cells as proof-of-concept

The OCI-Ly7 cell line is derived from human B-cell lymphoma cells in the bone marrow of a patient suffering from DLBCL (98). These cells grow in suspension as large clusters and have a doubling time of 23-28 h. They are considered as hard-to-transfect cells, but they are transducable with lentiviral vectors (81). However, based on the drawbacks with lentiviral production and the challenges of OCI-Ly7 plasmid transfection, HEK293T cells were chosen for the knockout experiments instead, since they are be transfected very efficiently with plasmid DNA (99) and transfection with plasmids had already been optimized in this cell line. HEK293 cells are adherent cells derived from modified human embryonic kidney cells. Further modification through stable transfection with SV40 large T antigen has led to the generation of the HEK293T cell line (100). This modification allows for episomal replication of plasmids containing the SV40 origin of replication, thus permitting a sustained recombinant protein production (99).

Generation and selection of monoclonal *WEE1* knockout cells prior to functional assays is favorable, as it allows for direct comparison between a specific genotype and phenotype. As the indels generated by the CRISPR/Cas9 system vary between cells in culture, monoclonal selection is optimal. However as this does not guarantee the generation of homozygotic knockout cells (gene knockout of both alleles in diploid cells) further selection and sequencing is needed. However, as the generation of monoclonal, biallelic knockout cells is a highly time-consuming task, heterogenous cell populations containing *WEE1* knockout cells were utilized for the initial experiments in this project as proof-of-concept for the study aim.

4.3 *WEE1* gene expression after transfection

The sgRNA containing plasmids targeting *WEE1* were transfected into HEK293T cells to induce a knockout. Positively transfected cells were puromycin selected, and the *WEE1* mRNA expression of the heterogenous *WEE1* knockout cell populations was assessed alongside control cells. Surprisingly, ddPCR revealed that the relative expression of *WEE1* mRNA was higher for all sgRNA transfected populations. Closer examination showed that the highest relative expression was seen in the sgGamma transfected cell population, which interestingly also displayed the lowest indel frequency and KO scores. The lowest expression was seen in the sgAlpha population and were almost as low as the mRNA expressions seen sgControl population and HEK293T WT cells. It is however noteworthy, that these results represent findings from a heterogenous mix of *WEE1* knockout cells, in which most of the cells did not have a knockout of *WEE1* as shown by the KO scores. In addition, these samples were only run once, and despite the high accuracy and precision of ddPCR (101), having multiple biological replicates from each population would more precisely display the variations in the relative expression of *WEE1* within each heterogenous cell population.

The higher expressions of sgBeta in comparison to sgAlpha, and sgDelta in comparison to sgGamma can possibly be explained by non-sense mediated mRNA decay (NMD). NMD is an eukaryotic quality inspection of mRNA, where edited transcripts containing a premature termination codon (PTC), that would otherwise lead to a truncated protein, triggers mRNA destruction. These transcripts are destroyed within one minute by NMD after they are exported from the nucleus to the cytoplasm. However, the transcripts are only considered NMD-sensitive if the PTC resides ≥ 50-55 nt upstream of an exon-exon junction, as this is the general indication that the stop codon is premature whereby mRNA can be fragmented and destroyed by exoribonucleases. (102,103)

The cut sites for sgBeta and sgGamma targets are 37 nt and 11 nt upstream of the exon-exon junction respectively (supplementary figure 11), whereby NMD mediated destruction of the mRNA transcripts is not possible, and the transcripts are thus NMD-resistant. However, as the cut sites for sgAlpha and sgDelta lie 190 nt and 189 nt upstream of the exon-exon junction respectively, the formation of a PTC as a consequence of genome editing in the region ≥ 50-55 nt upstream of an exon-exon junction, is possible. This could attribute to the increased *WEE1* mRNA levels in sgBeta and sgGamma populations as detected by ddPCR and highlights the importance of a strategic approach in choosing the targeting region for sgRNAs in an exon.

Another phenomenon observed in studies using CRISPR/Cas9 is unexpected exon skipping/non-sense mediated alternative splicing subsequent to Cas9-induced indels (104–106). When Cas9 induces DSBs and PTCs are consequently created, transcripts can be alternatively spliced, so they no longer contain the PTC in the exon (exon skipping) (105). This response can upregulate alternatively spliced mRNAs which might result in the production of aberrant proteins (106). The triggering mechanism behind this phenomenon is still not fully understood, however it has previously been demonstrated that CRISPR/Cas9-associated genome editing, which result in PTC mutations in exons other than exon 1, leads to exon skipping at high frequencies (106). However, exon skipping did not occur in the case of non-frameshift mutations or missense mutations, thus exon skipping is not dependent on an indel or DNA damage but only PTCs (105,106). This phenomenon could be investigated by conducting a RT-PCR reaction using primers that target exon 1 and exons downstream of exon 2 on cDNA from *WEE1* mRNA (104). Gel electrophoresis could then reveal whether amplicon size has changed as a result of exon skipping.

In summary, as all sgRNAs used in this study target exon 2, non-sense mediated alternative splicing subsequent to the PTC generation or exon skipping cannot be excluded and could therefore partially explain increased mRNA levels subsequent to *WEE1* knockout in the heterogenous cell populations.

Lastly, in addition to measuring the *WEE1* mRNA level, a determination of WEE1 protein expression is also of importance when explaining the effect of WEE1 in vincristine resistance, as the functional kinase property of WEE1 is on the protein level (56). Hereby the efficiency of each sgRNA in causing both a genomic and functional knockout could be assessed e.g. through western blot analysis (92).

4.4 Cell cycle analysis

Given the role of *WEE1* in G2-M phase transition, a cell cycle analysis of the sgRNA transfected cells and controls was conducted on cell cultures at 60-70% confluency. In accordance with previous assays, cell cycle analysis was performed separately for each stage of transfection (sgAlpha, sgBeta, and HEK293T WT cell populations from the first stage, and sgGamma, sgDelta, and sgControl cell population from the second stage). The cells were fixed in 70% ethanol and four replicates of 1 mio. cells were stained with PI and analyzed. However, a substantial cell loss during the preparation for cell cycle analysis was observed after each centrifugation step and resulted in low cell counts during flow cytometry analysis of cells from both transfections. Therefore, all replicates were combined and analyzed at once. Despite this, the range of 20,372 – 43,362 cells run through the flow cytometer could not be analyzed by the Watson (pragmatic) or Dean-Jett-Fox cell cycle models included in FlowJo software, thus gating for each cell cycle phase was performed manually. The cell loss might be due to improper fixation, and a change in the fixation methods to formaldehyde might be better, as this did not cause any cell loss previously when used for the transduced OCI-Ly7 cells and has been reported to be better when measuring highly fragmented DNA (sub-G1) (107).

The sgAlpha and sgBeta transfected cells from the first transfection accumulated slightly more in the G1 phase when compared to HEK293T WT cells. More cells were also seen in the sub-G1 phase for these transfected cells. This is in accordance with previous findings using WEE1 inhibitors (500 nM MK-1775) for 48h on ethanol fixed acute myeloid leukemia cell lines. Here, cell cycle analysis of PI stained cells showed that WEE1 inhibition abrogated G2/M cell cycle checkpoint and caused an increase in the sub-G1 population (108). Despite the results in the cell populations from the first transfection, the sgGamma, sgDelta, and sgControl cell populations from the second transfection did not display a substantial difference in the cell cycle phases. However, once again it is worth emphasizing that the *WEE1* knockout cell populations were heterogenous, and WEE1 protein might therefore still be expressed.

In addition to PI staining, other markers of the different cell cycle phases exist. PI is a fluorescent intercalating agent, that binds to all DNA content within the cells. By using bromodeoxyuridine (BrdU) labelling, cell proliferation can be detected, as BrdU is a synthetic nucleoside analogous to thymidine and gets incorporated into the DNA of replicating cells during the S phase. Actively replicating cells can then be detected by flowcytometry or immunofluorescence imaging by use of anti-BrdU antibodies. By combining BrdU with PI staining, cells in S phase can be clearly separated from cells in G1- and G2/M phase, and the cell cycle phases of transfected cells can be better

characterized. (109,110) Additionally, cell cycle analysis can be conducted through immunofluorescence by using antibodies against specific proteins expressed during each phase of the cell cycle. In *WEE1* deficient cells, mitotic events have been investigated using antibodies targeting phosphorylation of serine 10 on histone-H3 (a commonly used marker for mitosis), Aurora B (a mitotic marker), and phosphorylation of p27 (marks the G1/S transition), and could also be used to better characterize the cell cycle of the transfected cells in this project (42).

4.5 Vincristine response in *WEE1* knockout cells

In addition to the characterization assays, functional assays consisting of vincristine dose-response experiments was also conducted. The response to vincristine was investigated in heterogenous HEK293T cell populations with CRISPR/Cas9 induced knockout of *WEE1*. These were compared to a sgRNA transfected control population (sgControl) and HEK293T WT cells. The vincristine dose-response assay was performed in two stages in line with the two-step generation of sgRNA transfected cell populations. Due to variations on multiple parameters between the two transfections of the different cell populations (e.g. the length of puromycin treatment for selection and types of control), results are discussed separately.

For the first transfection, the HEK293T WT cells proved to be significantly more sensitive to vincristine treatment when compared to the sgAlpha and sgBeta populations, and the dose-response curve in the vincristine assay was similar to a test run conducted earlier using the same vincristine concentrations. However, HEK293T cells are not the most optimal vincristine treatment controls, as the *WEE1* knockout populations have undergone several handling and manipulative steps prior to vincristine treatment, which might have influenced the vincristine response. These include chemical transfection with calcium phosphate, expression of recombinant proteins in the plasmid cassette, and puromycin treatment which may affect cellular processes and impact the outcome of subsequent experimental studies (82). The differences between the HEK293T WT control and the transfected cell populations are highlighted in the cell counting assay, where it could be seen, that the sgAlpha and sgBeta transfected cell populations had a lower rate of proliferated than the HEK2933T WT cells. This could contribute to the higher vincristine induced growth inhibition seen in HEK293T WT cells, since they proliferated at a higher rate and vincristine kills dividing cells during the M phase as previously described (15). In addition it has also been observed that there is an inherent bias in drug response between slow and fast growing cells, wherein fast growing cells are considered more sensitive (111). It can therefore not be concluded, whether the differences in growth inhibition between the HEK293T cell population and the sgAlpha and sgBeta populations are due to vincristine

or other factors in the experimental setup, and better controls are therefore needed for more accurate interpretation.

Transfection with sgControl is the best treatment control when using the sgRNAs targeting *WEE1* and was therefore included in the second transfection. Here, the heterogenous sgDelta transfected population displayed a significant vincristine induced growth inhibition when compared the sgGamma and sgControl populations at higher concentrations. Furthermore, the highest indel frequency and KO-score was also observed in the sgDelta population. In addition, the sgGamma population, which had lower indel frequency and KO-score, also displayed increased vincristine sensitivity at higher concentrations when compared to the unedited sgControl population. As the three cell populations were parallel transfected, cultured and assayed alongside each other, the only difference remaining between the sgRNA transfected cell populations is the frequencies of *WEE1* knockout. Taken together these finding suggest that knockout of *WEE1* in heterogenous HEK293T cell populations increase sensitivity to higher concentrations of vincristine.

These results support previous observations using chemical inhibition of WEE1. In a study by *Due et al.* WEE1 inhibition (400 nM MK-1775) resulted in increased vincristine sensitivity in the vincristine resistant DLBCL cells line, OCI-Ly7 (85). Increased apoptotic cell death after chemical WEE1 inhibition (10-20 nM MK-1775) in combination with vincristine has also been observed in two acute lymphoblastic leukemia (ALL) cell lines (58). Similar results have been found when combining the WEE1 inhibitor with doxorubicin (topoisomerase II inhibitor), which is another component of the R-CHOP treatment in DLBCL. Cells treated with a WEE1 inhibitor (100 nM MK-1775) potentiated the cytotoxic effects of doxorubicin in B-cell lymphomas (52), ALL cell lines (6-5000 nM MK-1775) (45), and colon cancer cells (100-300 nM MK-1775) (57). Additionally, WEE1 inhibition (200-2000 nM MK-1775) has also been found to increase the cytotoxic effect of rituximab, another component of the R-CHOP combination treatment, in eight DLBCL cell lines (44). Taken together, these findings indicate that targeting WEE1 sensitize DLBCL cells, as well as other cancer cells, to immuno- and chemotherapy treatment.

In this study, chemical inhibition of WEE1 using 125 nM MK-1775 did not cause HEK293T cells to become more sensitive to vincristine. Perhaps this concentration was suboptimal to obtain inhibition of WEE1, as the abovementioned studies using MK-1775 did find that cells became more sensitive to the effects of chemotherapeutic treatment. In addition, treatment with MK-1775 alone causes apoptosis in AML and DLBCL cell lines, including the OCI-Ly7, to a lesser extent than when

combined with other drugs (85,108). As 125 nM MK-1775 did not cause growth inhibition by itself, the concentration used might not have been high enough to inhibit WEE1. An assessment of the WEE1 protein expression (e.g. through western blot) after treatment with the large range of MK-1775 concentrations used prior to the double drug assay could provide better information of the optimal MK-1775 concentration needed to inhibit WEE1 in the HEK293T cells.

4.6 Limitations

There are some limitations in this study. First and foremost, all sgRNAs were designed to target exon 2 in *WEE1*. This exon was chosen, as it is generally recommended by all the used designing tools to choose an early consecutive exon present in all splice variants. However, despite targeting exon 2 in *WEE1*, which consists of the same DNA sequence in both *WEE1* transcript variants, sgAlpha and sgDelta only targets the coding sequence (CDS) of transcript variant 1 (NM_003390.3), whereas they target the 5' untranslated region (UTR) on transcript variant 2 (NM_001143976.1) (illustrated on supplementary figure 11). This is due to the fact, that the 5' UTR spans over the first two exons for transcript variant 2, but not for transcript variant 1. As sgBeta and sgGamma target further downstream on exon 2, their target sites are within the CDS region for both transcript variants (29). Since 5'UTRs lie directly upstream from the initiation codon (AUG) of the CDS, they are not a part of the final protein product (112). However, it has previously been suggested that WEE1 isoform 2 (a 49 kDa isoform translated from transcript variant 2 lacking the inhibitory NH_2-terminal domain) might not be expressed in humans, as it could not be detected by western blot analysis in human cell lines in contrast to rat and murine cell lines where it was expressed (113,114).

Contrary to these findings, the degradation product of WEE1 with a similar size as isoform 2 has been observed in tissues obtained from Alzheimer Disease patients (115). However, it was not confirmed whether this was from transcript variant 2 as it was described as the degradation product from proteolysis of WEE1. In addition, mRNA expression of both transcript variants has been observed in human prostate adenocarcinoma cells, and could be downregulated using androgen treatment, however protein expression was not investigated in that study (116). Thus, it is not known whether the protein product of transcript variant 2 is expressed in the transfected cell populations nor whether it had an impact on vincristine response in the sgAlpha and sgDelta transfected cell populations.

Another limitation is the puromycin selection process of cells from the second transfection. Cloned plasmids were found in the HEK293T WT controls cells, and this was possibly caused by contamination with plasmid containing cells. Since the HEK293T WT cells were used as indicators

for puromycin selection, the selection of transfected cells could not be completed properly, and non-transfected cells might therefore still be present in the selected sgGamma, sgDelta, and sgControl cell populations. Despite this, experimental assays were conducted using these cells, since the HEK293T WT control cells could no longer indicate when selection of transfected cells was complete. LentiCRISPR v2 was originally chosen due to the possibility of puromycin selection after lentiviral transduction of OCI-Ly7 cells. Selection of positively transfected cells using eGFP as a selection marker was not possible, as a fluorescence-activated cell sorter (FACS) suited for work with live cells containing lentivirus was not available. However, since HEK293T cells were used for the knockout experiments instead, an eGFP containing plasmid could alternatively be used for cloning, transfection and subsequent selection rather than LentiCRISPR v2. This might overcome the challenges experienced with puromycin selection and be timesaving as well. However, as eGFP containing plasmids would not be applicable for subsequent work with lentiviral vectors and OCI-Ly7 in this study, using two different selection markers (eGFP for HEK293T and puromycin resistance for OCI-Ly7) might complicate comparisons between results obtained using the two cell lines.

4.7 Future perspectives

To assess the role of *WEE1* in vincristine resistance, a heterogenous mix of *WEE1* knockout HEK293T cells was used in this study. The assays conducted should initially be repeated in monoclonal and homozygotic *WEE1* knockout HEK293T cells. WEE1 protein expression should also be assessed to verify that CRISPR/Ca9 has induced functional knockout of the *WEE1* gene. Additional experiments such cell cycle analysis using other markers, and analysis of DNA damage would be interesting to investigate since aberrant mitosis has been observed after knockout of *WEE1* (42). In addition to technical replicates within each assay, experiments should be performed in biological replicates to strengthen the evidence and the biological interpretation for all findings.

As vincristine resistance in DLBCL is the focus of this study, these assays should be repeated in the vincristine resistant DLBCL cell lines like OCI-Ly7 as originally intended, using the results obtained from HEK293T cells as comparison. OCI-Ly7 is of special interest since it has previously been found to lack functional p53 protein (117), whereby they rely more on the G2/M checkpoint after DNA damage (50). Thus, knockout of *WEE1* might result in simultaneous aberration of both the G1 checkpoint and the G2/M checkpoint in these cells, further disrupting the genetic integrity and possibly sensitize the cells to vincristine treatment. In addition to OCI-Ly7, there are other vincristine resistant DLBCL cell lines such as SU-DHL-8 and DB cell lines (85). It would similarly be interesting to investigate the role of *WEE1* in vincristine response in these cell lines and compare the findings to

vincristine sensitive cell lines of both the ABC and GCB DLBCL subclasses. A comparison between the vincristine response and the expression of *WEE1* in the various DLBCL cell lines could be important to determine whether *WEE1* has a biomarker potential for R-CHOP response in DLBCL. In addition to vincristine, the effects of *WEE1* knockout on other drugs in the R-CHOP regimen would be interesting to investigate, as chemical WEE1 inhibition has previously been shown, to sensitize cells to other immune- and chemotherapeutic drugs (44,45).

Next, findings from the experiments conducted on DLBCL cell lines, could be used to improve risk stratification tools in primary clinical DLBCL cohorts. The biomarker potential for *WEE1* and possible resistance mechanisms identified should be assessed in local retrospective clinical cohort of diagnostic DLBCL and relapsed DLBCL. This could be tested for association to clinical prognostic parameters, molecular subtypes, genetic profiles and outcome, as previously done in the assessment of miR-155 as a biomarker for DLBCL (85). This can be performed using tissues from R-CHOP treated patients with available clinical follow-up or using available data hereof, such as gene expression profiles, whole exome sequencing, and RNA sequencing data from diagnostic and relapsed DLBCL. Lastly, the potential risk stratification of *WEE1* identified in local cohort could be expanded to larger in silico cohorts for validation in order to identify cases where patients would benefit the most of alternative treatment.

5. Conclusion

In this study, the role of *WEE1* in vincristine resistance was investigated. Four sgRNAs targeting the *WEE1* gene were cloned into CRISPR/Cas9 plasmid constructs and insertion was verified through PCR and Sanger sequencing. The sgRNA containing plasmids were transfected into HEK293T cells where they induced indel mutations in *WEE1*, resulting in the generation of four bulk *WEE1* knockout cells. ICE analysis revealed editing efficiencies over 50% for all cell populations and indicated that all sgRNAs induced knockout of *WEE1* with varying efficiencies.

Characterization assays revealed slower growth of transfected cells subsequent puromycin selection. Flow cytometry analysis did not indicate a change in cell cycle phases, however droplet digital PCR indicated higher relative expression of *WEE1* mRNA in cell populations transfected with *WEE1* targeting sgRNAs. Vincristine treatment at higher concentrations resulted in significant growth inhibition in heterogenous cell populations transfected with sgRNAs targeting *WEE1* in comparison to cells transfected with non-targeting sgRNAs. In summary, these results indicate that CRISPR/Cas9 mediated knockout of *WEE1* can increase vincristine sensitivity in resistant DLBCL cells, suggesting that *WEE1* plays an important role in drug resistance in DLBCL.

6. References

1. Swerdlow SH, Campo E, Pileri SA, Harris NL, Stein H, Siebert R, et al. The 2016 revision of the World Health Organization classification of lymphoid neoplasms. Blood [Internet]. 2016 May 19;127(20):2375–90. Available from: http://dx.doi.org/10.1053/j.ajkd.2013.01.026

2. Hanahan D, Weinberg RA. Hallmarks of Cancer: The Next Generation. Cell [Internet]. 2011 Mar;144(5):646–74. Available from: http://dx.doi.org/10.1016/j.cell.2011.02.013

3. Ninkovic S, Lambert J. Non-Hodgkin lymphoma. Medicine (Baltimore) [Internet]. 2017 May;45(5):297–304. Available from: http://dx.doi.org/10.1016/S0140-6736(12)60605-9

4. Martelli M, Ferreri AJM, Agostinelli C, Di Rocco A, Pfreundschuh M, Pileri SA. Diffuse large B-cell lymphoma. Crit Rev Oncol Hematol [Internet]. 2013;87(2):146–71. Available from: http://dx.doi.org/10.1016/j.critrevonc.2012.12.009

5. RKKP A for KE og B i. Malignt Lymfom og CLL National årsrapport 2016 [Internet]. Den landsdækkende LYFO database. 2016. p. 1–73. Available from: http://www.lymphoma.dk/wp-content/uploads/2017/11/Årsrapport_LYFO-og-CLL-2016_endelig.pdf

6. Li S, Young KH, Medeiros LJ. Diffuse large B-cell lymphoma. Pathology [Internet]. 2018 Jan 30;50(1):74–87. Available from: https://www.taylorfrancis.com/books/9781444113228

7. Dockery DW, Pope III CA, Xu X, Spengler JD, Ware JH, Fay ME, et al. A Predictive Model for Aggressive Non-Hodgkin's Lymphoma. N Engl J Med [Internet]. 1993 Sep 30;329(14):987–94. Available from: http://www.nejm.org/doi/abs/10.1056/NEJM199309303291402

8. Alizadeh AA, Alizadeh AA, Eisen MB, Eisen MB, Davis RE, Davis RE, et al. Distinct types of diffuse large B-cell lymphoma identified by gene expression profiling. Nature. 2000;403(6769):503–11.

9. Visco C, Li Y, Xu-Monette ZY, Miranda RN, Green TM, Li Y, et al. Comprehensive gene expression profiling and immunohistochemical studies support application of immunophenotypic algorithm for molecular subtype classification in diffuse large B-cell lymphoma: A report from the International DLBCL Rituximab-CHOP Consortiu. Leukemia. 2012;26(9):2103–13.

10. Sehn LH, Donaldson J, Chhanabhai M, Fitzgerald C, Gill K, Klasa R, et al. Introduction of combined CHOP plus rituximab therapy dramatically improved outcome of diffuse large B-cell lymphoma in British Columbia. J Clin Oncol. 2005;23(22):5027–33.

11. Vaidya R, Witzig TE. Prognostic factors for diffuse large B-cell lymphoma in the R(X)CHOP era. Ann Oncol [Internet]. 2014 Nov 1;25(11):2124–33. Available from: https://academic.oup.com/annonc/article-lookup/doi/10.1093/annonc/mdu109

12. Liu Y, Barta SK. Diffuse large B-cell lymphoma: 2019 update on diagnosis, risk stratification, and treatment. Am J Hematol [Internet]. 2019 May 4;94(5):604–16. Available from: https://onlinelibrary.wiley.com/doi/abs/10.1002/ajh.25460

13. Zheng X, Ding N, Song Y, Feng L, Zhu J. Different sensitivity of germinal center B cell-like diffuse large B cell lymphoma cells towards ibrutinib treatment. Cancer Cell Int [Internet]. 2014;14(1):32. Available from: http://cancerci.biomedcentral.com/articles/10.1186/1475-2867-14-32

14. Gidding C. Vincristine revisited. Crit Rev Oncol Hematol [Internet]. 1999 Feb;29(3):267–87. Available from: https://linkinghub.elsevier.com/retrieve/pii/S1040842898000237

15. Jordan M. Mechanism of Action of Antitumor Drugs that Interact with Microtubules and Tubulin. Curr Med Chem Agents. 2005;2(1):1–17.

16. Jordan MA, Thrower D, Wilson L. Mechanism of inhibition of cell proliferation by Vinca alkaloids. Cancer Res [Internet]. 1991 Apr 15;51(8):2212–22. Available from: http://www.ncbi.nlm.nih.gov/pubmed/2009540

17. Johnson NA, Slack GW, Savage KJ, Connors JM, Ben-Neriah S, Rogic S, et al. Concurrent expression of MYC and BCL2 in diffuse large B-cell lymphoma treated with rituximab plus cyclophosphamide, doxorubicin, vincristine, and prednisone. J Clin Oncol. 2012;30(28):3452–9.

18. Johnson N a, Savage KJ, Ludkovski O, Ben-Neriah S, Woods R, Steidl C, et al. Lymphomas with concurrent BCL2 and MYC translocations: the critical factors associated with survival. Blood [Internet]. 2009 Sep 10;114(11):2273–9. Available from: http://www.bloodjournal.org/cgi/doi/10.1182/blood-2009-03-212191

19. Greenblatt MS, Bennett WP, Hollstein M, Harris CC. Mutations in the p53 tumor suppressor gene: clues to cancer etiology and molecular pathogenesis. Cancer Res [Internet]. 1994 Sep 15;54(18):4855–78. Available from: http://www.ncbi.nlm.nih.gov/pubmed/8069852

20. Vermeulen K, Van Bockstaele DR, Berneman ZN. The cell cycle: a review of regulation, deregulation and therapeutic targets in cancer. Cell Prolif [Internet]. 2003 Jun;36(3):131–49. Available from: https://pubs.geoscienceworld.org/jsedres/article/36/4/973-976/95989

21. Xu-Monette ZY, Wu L, Visco C, Tai YC, Tzankov A, Liu W -m., et al. Mutational profile and prognostic significance of TP53 in diffuse large B-cell lymphoma patients treated with R-CHOP: report from an International DLBCL Rituximab-CHOP Consortium Program Study. Blood [Internet]. 2012 Nov 8;120(19):3986–96. Available from: http://www.bloodjournal.org/cgi/doi/10.1182/blood-2012-05-433334

22. Voropaeva EN, Pospelova TI, Voevoda MI, Maksimov VN. Frequency, spectrum, and functional significance of TP53 mutations in patients with diffuse large B-cell lymphoma. Mol Biol [Internet]. 2017 Jan 23;51(1):53–60. Available from: http://link.springer.com/10.1134/S0026893316060224

23. Zhang J, Grubor V, Love CL, Banerjee A, Richards KL, Mieczkowski PA, et al. Genetic heterogeneity of diffuse large B-cell lymphoma. Proc Natl Acad Sci [Internet]. 2013 Jan 22;110(4):1398–403. Available from: http://www.nature.com/doifinder/10.1038/sj.thj.6200441

24. Sun R, Wang J, Young KH. Oncogenic Signaling Pathways and Pathway-Based Therapeutic Biomarkers in Lymphoid Malignancies. Crit Rev Oncog [Internet]. 2017;22(5–6):527–57. Available from: http://www.dl.begellhouse.com/journals/439f422d0783386a,5fec323e07ab6bc2,485adf5503f1ae40.html

25. Otto T, Sicinski P. Cell cycle proteins as promising targets in cancer therapy. Nat Rev Cancer [Internet]. 2017;17(2):93–115. Available from: http://dx.doi.org/10.1038/nrc.2016.138

26. Nurse P, Thuriaux P. Regulatory genes controlling mitosis in the fission yeast Schizosaccharomyces pombe. Genetics. 1980;96(3):627–37.

27. Igarashi M, Nagata A, Jinno S, Suto K, Okayama H. Wee1+-like gene in human cells. Nature [Internet]. 1991 Sep;353(6339):80–3. Available from: http://www.nature.com/articles/353080a0

28. Taviaux SA, Demaille JG. Localization of Human Cell Cycle Regulatory Genes CDC25C to 5q31 and WEE1 to 11p15.3-11p15.1 by Fluorescence in Situ Hybridization. Genomics [Internet]. 1993 Jan;15(1):194–6. Available from: https://linkinghub.elsevier.com/retrieve/pii/S0888754383710323

29. National Center for Biotechnology Information (NCBI). Wee1 gene [Internet]. 2019 [cited 2019 Mar 13]. Available from: https://www.ncbi.nlm.nih.gov/gene/7465

30. Morgan Do. Principles of CDK regulation. Nature. 1995;374(6518):131–4.

31. Nigg EA. Mitotic kinases as regulators of cell division and its checkpoints. Nat Rev Mol Cell Biol [Internet]. 2001 Jan;2(1):21–32. Available from: http://www.nature.com/articles/35048096

32. Lindqvist A, Rodríguez-Bravo V, Medema RH. The decision to enter mitosis: feedback and redundancy in the mitotic entry network. J Cell Biol [Internet]. 2009 Apr 20;185(2):193–202. Available from: http://www.jcb.org/lookup/doi/10.1083/jcb.200812045

33. Peters J. The anaphase promoting complex/cyclosome: a machine designed to destroy. Nat Rev Mol Cell Biol [Internet]. 2006 Sep 9;7(9):644–56. Available from: http://www.nature.com/articles/nrm1988

34. Musacchio A, Salmon ED. The spindle-assembly checkpoint in space and time. Nat Rev Mol Cell Biol [Internet]. 2007 May 11;8(5):379–93. Available from: http://www.nature.com/articles/nrm2163

35. Connell MJO, Raleigh JM, Verkade HM, Nurse P. Chk1 is a wee1 kinase in the G 2 DNA damage checkpoint inhibiting cdc2 by Y15 phosphorylation. 1997;16(3):545–54.

36. Harvey SL, Charlet A, Haas W, Gygi SP, Kellogg DR. Cdk1-Dependent Regulation of the Mitotic Inhibitor Wee1. Cell [Internet]. 2005 Aug;122(3):407–20. Available from: https://linkinghub.elsevier.com/retrieve/pii/S0092867405005507

37. Chow JPH, Poon RYC, Ma HT. Inhibitory Phosphorylation of Cyclin-Dependent Kinase 1 as a Compensatory Mechanism for Mitosis Exit. Mol Cell Biol [Internet]. 2011 Apr 1;31(7):1478–91. Available from: http://mcb.asm.org/cgi/doi/10.1128/MCB.00891-10

38. Malumbres M, Barbacid M. Mammalian cyclin-dependent kinases. Trends Biochem Sci. 2005;30(11):630–41.

39. Chow JPH, Poon RYC. The CDK1 inhibitory kinase MYT1 in DNA damage checkpoint recovery. Oncogene [Internet]. 2013 Oct 12;32(40):4778–88. Available from: http://dx.doi.org/10.1038/onc.2012.504

40. Kellogg DR. Wee1-dependent mechanisms required for coordination of cell growth and cell division. J Cell Sci. 2003;116(24):4883–90.

41. Tominaga Y, Li C, Wang R-H, Deng C-X. Murine Wee1 plays a critical role in cell cycle regulation and pre-implantation stages of embryonic development. Int J Biol Sci [Internet]. 2006;2(4):161–70. Available from: http://www.ncbi.nlm.nih.gov/pubmed/16810330%0Ahttp://www.pubmedcentral.nih.gov/articlerender.fcgi?artid=PMC1483124

42. Vassilopoulos A, Tominaga Y, Kim HS, Lahusen T, Li B, Yu H, et al. WEE1 murine deficiency induces hyper-activation of APC/C and results in genomic instability and carcinogenesis. Oncogene. 2015;34(23):3023–35.

43. De Witt Hamer PC, Mir SE, Noske D, Van Noorden CJF, Würdinger T. WEE1 kinase targeting combined with DNA-damaging cancer therapy catalyzes mitotic catastrophe. Clin Cancer Res. 2011;17(13):4200–7.

44. de Jong MRW, Visser L, Huls G, Diepstra A, van Vugt M, Ammatuna E, et al. Identification of relevant drugable targets in diffuse large B-cell lymphoma using a genome-wide unbiased CD20 guilt-by association approach. Bertolini F, editor. PLoS One [Internet]. 2018 Feb 28;13(2):e0193098. Available from: https://dx.plos.org/10.1371/journal.pone.0193098

45. Ghelli Luserna Di Rorà A, Beeharry N, Imbrogno E, Ferrari A, Robustelli V, Righi S, et al. Targeting WEE1 to enhance conventional therapies for acute lymphoblastic leukemia. J Hematol Oncol [Internet]. 2018 Dec 1;11(1):99. Available from: https://jhoonline.biomedcentral.com/articles/10.1186/s13045-018-0641-1

46. Magnussen GI, Holm R, Emilsen E, Rosnes AKR, Slipicevic A, Flørenes VA. High expression of Wee1 is associated with poor disease-free survival in Malignant Melanoma: Potential for targeted therapy. PLoS One. 2012;7(6):1–8.

47. Kiviharju-af Hallstrom TM, Jaamaa S, Monkkonen M, Peltonen K, Andersson LC, Medema RH, et al. Human prostate epithelium lacks Wee1A-mediated DNA damage-induced checkpoint enforcement. Proc Natl Acad Sci [Internet]. 2007 Apr 24;104(17):7211–6. Available from: http://www.pnas.org/cgi/doi/10.1073/pnas.0609299104

48. Yoshida T, Tanaka S, Mogi A, Shitara Y, Kuwano H. The clinical significance of Cyclin B1 and Wee1 expression in non-small-cell lung cancer. Ann Oncol. 2004;15(2):252–6.

49. Backert S, Gelos M, Kobalz U, Hanski ML, Böhm C, Mann B, et al. Differential gene expression in colon carcinoma cells and tissues detected with a cDNA array. Int J Cancer. 1999;82(6):868–74.

50. Hirai H, Iwasawa Y, Okada M, Arai T, Nishibata T, Kobayashi M, et al. Small-molecule inhibition of Wee1 kinase by MK-1775 selectively sensitizes p53-deficient tumor cells to DNA-damaging agents. Mol Cancer Ther [Internet]. 2009 Nov 1;8(11):2992–3000. Available from: http://mct.aacrjournals.org/cgi/doi/10.1158/1535-7163.MCT-09-0463

51. Denisenko T V., Sorokina I V., Gogvadze V, Zhivotovsky B. Mitotic catastrophe and cancer drug resistance: A link that must to be broken. Drug Resist Updat [Internet]. 2016 Jan;24:1–12. Available from: http://dx.doi.org/10.1016/j.drup.2015.11.002

52. Wang X, Chen Z, Mishra AK, Silva A, Ren W, Pan Z, et al. Chemotherapy-induced differential cell cycle arrest in B-cell lymphomas affects their sensitivity to Wee1 inhibition. Haematologica [Internet]. 2018 Mar;103(3):466–76. Available from: http://www.haematologica.org/lookup/doi/10.3324/haematol.2017.175992

53. Castedo M, Perfettini J-L, Roumier T, Andreau K, Medema R, Kroemer G. Cell death by mitotic catastrophe: a molecular definition. Oncogene [Internet]. 2004 Apr 12;23(16):2825–37. Available from: http://www.ncbi.nlm.nih.gov/pubmed/15077146

54. Matheson CJ, Backos DS, Reigan P. Targeting WEE1 Kinase in Cancer. Trends Pharmacol Sci [Internet]. 2016 Oct;37(10):872–81. Available from: http://dx.doi.org/10.1016/j.tips.2016.06.006

55. Lescarbeau RS, Lei L, Bakken KK, Sims PA, Sarkaria JN, Canoll P, et al. Quantitative Phosphoproteomics Reveals Wee1 Kinase as a Therapeutic Target in a Model of Proneural Glioblastoma. Mol Cancer Ther [Internet]. 2016 Jun;15(6):1332–43. Available from: http://mct.aacrjournals.org/lookup/doi/10.1158/1535-7163.MCT-15-0692-T

56. Do K, Doroshow JH, Kummar S. Wee1 kinase as a target for cancer therapy. Cell Cycle [Internet]. 2013 Oct 29;12(19):3348–53. Available from: http://www.tandfonline.com/doi/full/10.1517/13543784.2012.668527

57. Hirai H, Arai T, Okada M, Nishibata T, Kobayashi M, Sakai N, et al. MK-1775, a small molecule Wee1 inhibitor, enhances anti-tumor efficacy of various DNA-damaging agents, including 5-fluorouracil. Cancer Biol Ther [Internet]. 2010 Apr 27;9(7):514–22. Available from: http://www.tandfonline.com/doi/abs/10.4161/cbt.9.7.11115

58. Visconti R, Della Monica R, Palazzo L, D'Alessio F, Raia M, Improta S, et al. The Fcp1-Wee1-Cdk1 axis affects spindle assembly checkpoint robustness and sensitivity to antimicrotubule cancer drugs. Cell Death Differ [Internet]. 2015 Sep 6;22(9):1551–60. Available from: http://www.nature.com/articles/cdd201513

59. Murrow LM, Garimella S V., Jones TL, Caplen NJ, Lipkowitz S. Identification of WEE1 as a potential molecular target in cancer cells by RNAi screening of the human tyrosine kinome. Breast

Cancer Res Treat [Internet]. 2010 Jul 10;122(2):347–57. Available from: http://link.springer.com/10.1007/s10549-009-0571-2

60. Iorns E, Lord CJ, Grigoriadis A, McDonald S, Fenwick K, MacKay A, et al. Integrated Functional, Gene Expression and Genomic Analysis for the Identification of Cancer Targets. Ouchi T, editor. PLoS One [Internet]. 2009 Apr 9;4(4):e5120. Available from: https://dx.plos.org/10.1371/journal.pone.0005120

61. Wright G, Golubeva V, Remsing Rix LL, Berndt N, Luo Y, Ward GA, et al. Dual Targeting of WEE1 and PLK1 by AZD1775 Elicits Single Agent Cellular Anticancer Activity. ACS Chem Biol [Internet]. 2017 Jul 21;12(7):1883–92. Available from: http://pubs.acs.org/doi/10.1021/acschembio.7b00147

62. Ishino Y, Shinagawa H, Makino K, Amemura M, Nakata A. Nucleotide sequence of the iap gene, responsible for alkaline phosphatase isozyme conversion in Escherichia coli, and identification of the gene product. J Bacteriol [Internet]. 1987 Dec;169(12):5429–33. Available from: http://jb.asm.org/lookup/doi/10.1128/jb.169.12.5429-5433.1987

63. Barrangou R, Fremaux C, Deveau H, Richards M, Boyaval P, Moineau S, et al. CRISPR Provides Acquired Resistance Against Viruses in Prokaryotes. Science (80-) [Internet]. 2007 Mar 23;315(5819):1709–12. Available from: http://www.sciencemag.org/cgi/doi/10.1126/science.1138140

64. Sun CL, Barrangou R, Thomas BC, Horvath P, Fremaux C, Banfield JF. Phage mutations in response to CRISPR diversification in a bacterial population. Environ Microbiol. 2013;15(2):463–70.

65. Barrangou R. The roles of CRISPR–Cas systems in adaptive immunity and beyond. Curr Opin Immunol [Internet]. 2015 Feb;32:36–41. Available from: http://dx.doi.org/10.1016/j.coi.2014.12.008

66. Jinek M, Chylinski K, Fonfara I, Hauer M, Doudna JA, Charpentier E. A Programmable Dual-RNA-Guided DNA Endonuclease in Adaptive Bacterial Immunity. Science (80-) [Internet]. 2012 Aug 17;337(6096):816–21. Available from: http://www.sciencemag.org/cgi/doi/10.1126/science.1225829

67. Cong L, Ran FA, Cox D, Lin S, Barretto R, Hsu PD, et al. Multiplex Genome Engineering Using CRISPR/VCas Systems. Science (80-). 2013;339(6121):819–23.

68. Makarova KS, Brouns SJJ, Horvath P, Sas DF, Wolf YI, Yakunin AF, et al. Evolution and classification of the CRISPR-Cas systems. Nat Rev Microbiol. 2011;9(6):467–77.

69. Chialva C, Eichler E, Muñoz C, Lijavetzky D. Development and Use of Biotechnology Tools for Grape Functional Analysis. In: Grape and Wine Biotechnology [Internet]. InTech; 2016. p. 13. Available from: http://www.intechopen.com/books/trends-in-helicobacter-pylori-infection/floating-drug-delivery-systems-for-eradication-of-helicobacter-pylori-in-treatment-of-peptic-ulcer-d

70. Cong L, Ran FA, Cox D, Lin S, Barretto R, Habib N, et al. Multiplex Genome Engineering Using CRISPR/Cas Systems. Science (80-) [Internet]. 2013 Feb 15;339(6121):819–23. Available from: http://www.sciencemag.org/cgi/doi/10.1126/science.1231143

71. Song M. The CRISPR/Cas9 system: Their delivery, in vivo and ex vivo applications and clinical development by startups. Biotechnol Prog [Internet]. 2017 Jul;33(4):1035–45. Available from: http://doi.wiley.com/10.1002/btpr.2484

72. Chapman JR, Taylor MRG, Boulton SJ. Playing the End Game: DNA Double-Strand Break Repair Pathway Choice. Mol Cell [Internet]. 2012;47(4):497–510. Available from: http://dx.doi.org/10.1016/j.molcel.2012.07.029

73. Kruminis-Kaszkiel E, Juranek J, Maksymowicz W, Wojtkiewicz J. CRISPR/Cas9 technology as an emerging tool for targeting amyotrophic lateral sclerosis (ALS). Int J Mol Sci. 2018;19(3).

74. Doudna JA, Charpentier E. The new frontier of genome engineering with CRISPR-Cas9. Science (80-) [Internet]. 2014 Nov 28;346(6213):1258096–1258096. Available from: http://www.sciencemag.org/cgi/doi/10.1126/science.1258096

75. Hsu PD, Lander ES, Zhang F. Development and Applications of CRISPR-Cas9 for Genome Engineering. Cell [Internet]. 2014 Jun;157(6):1262–78. Available from: http://dx.doi.org/10.1016/j.cell.2014.05.010

76. Cong L, Zhang F. Genome Engineering Using CRISPR-Cas9 System. In: Chromosomal Mutagenesis: Second Edition [Internet]. 2015. p. 197–217. Available from: http://link.springer.com/10.1007/978-1-4939-1862-1_10

77. Niu Y, Shen B, Cui Y, Chen Y, Wang J, Wang L, et al. Generation of Gene-Modified Cynomolgus Monkey via Cas9/RNA-Mediated Gene Targeting in One-Cell Embryos. Cell [Internet]. 2014 Feb;156(4):836–43. Available from: https://linkinghub.elsevier.com/retrieve/pii/S0092867414000798

78. Sojung Kim, Daesik Kim, Seung Woo Cho, Jungeun Kim J-SK. Highly efficient RNA-guided genome editing in human cells via delivery of purified Cas9 ribonucleoproteins. Genome Res. 2014;128:1–32.

79. DeWitt MA, Corn JE, Carroll D. Genome editing via delivery of Cas9 ribonucleoprotein. Methods [Internet]. 2017 May;121–122:9–15. Available from: https://linkinghub.elsevier.com/retrieve/pii/S1046202316302973

80. Liu C, Zhang L, Liu H, Cheng K. Delivery strategies of the CRISPR-Cas9 gene-editing system for therapeutic applications. J Control Release [Internet]. 2017 Nov;266(September):17–26. Available from: https://linkinghub.elsevier.com/retrieve/pii/S0168365917308453

81. Ranjbar B, Krogh LB, Laursen MB, Primo MN, Marques SC, Dybkær K, et al. Anti-apoptotic effects of lentiviral vector transduction promote increased Rituximab tolerance in cancerous B-cells. PLoS One. 2016;11(4):1–18.

82. Stepanenko AA, Heng HH. Transient and stable vector transfection: Pitfalls, off-target effects, artifacts. Mutat Res Mutat Res [Internet]. 2017 Jul;773:91–103. Available from: http://dx.doi.org/10.1016/j.mrrev.2017.05.002

83. Geraerts M, Willems S, Baekelandt V, Debyser Z, Gijsbers R. Comparison of lentiviral vector titration methods. BMC Biotechnol. 2006;6:1–10.

84. Milone MC, O'Doherty U. Clinical use of lentiviral vectors. Leukemia [Internet]. 2018 Jul 22;32(7):1529–41. Available from: http://dx.doi.org/10.1038/s41375-018-0106-0

85. Due H, Schonherz AA, Ryo LB, Roug AS, Johnsen HE, Bogsted M, et al. Microrna-155 controls vincristine sensitivity and predicts superior clinical outcome in diffuse large b-cell lymphoma. Basic Clin Pharmacol Toxicol [Internet]. 2018;123 (Suppl(7):12. Available from: http://ovidsp.ovid.com/ovidweb.cgi?T=JS&CSC=Y&NEWS=N&PAGE=fulltext&D=emexa&AN=622823904%0Ahttp://oxfordsfx.hosted.exlibrisgroup.com/oxford?sid=OVID:embase&id=pmid:&id=doi:&issn=1742-7843&isbn=&volume=123&issue=Supplement+1&spage=12&pages=12&date=2018&titl

86. Haeussler M, Schönig K, Eckert H, Eschstruth A, Mianné J, Renaud J-B, et al. Evaluation of off-target and on-target scoring algorithms and integration into the guide RNA selection tool CRISPOR. Genome Biol [Internet]. 2016 Dec 5;17(1):148. Available from: http://dx.doi.org/10.1186/s13059-016-1012-2

87. Labun K, Montague TG, Gagnon JA, Thyme SB, Valen E. CHOPCHOP v2: a web tool for the next generation of CRISPR genome engineering. Nucleic Acids Res. 2016;44(W1):W272–6.

88. Sanjana NE, Shalem O, Zhang F. Improved vectors and genome-wide libraries for CRISPR screening. Nat Methods [Internet]. 2014 Aug 1;11(8):783–4. Available from: http://www.nature.com/articles/nmeth.3047

89. Sander JD, Joung JK. CRISPR-Cas systems for editing, regulating and targeting genomes. Nat Biotechnol [Internet]. 2014 Apr 2;32(4):347–55. Available from: http://dx.doi.org/10.1038/nbt.2842

90. Walter DM, Venancio OS, Buza EL, Tobias JW, Deshpande C, Gudiel AA, et al. Systematic In Vivo Inactivation of Chromatin-Regulating Enzymes Identifies Setd2 as a Potent Tumor Suppressor in Lung Adenocarcinoma. Cancer Res [Internet]. 2017;77(7):1719–29. Available from: http://www.ncbi.nlm.nih.gov/pubmed/28202515

91. Schindelin J, Arganda-Carreras I, Frise E, Kaynig V, Longair M, Pietzsch T, et al. Fiji: an open-source platform for biological-image analysis. Nat Methods [Internet]. 2012 Jul 28;9(7):676–82. Available from: http://www.ncbi.nlm.nih.gov/pubmed/22743772%0Ahttp://www.pubmedcentral.nih.gov/articlerender.fcgi?artid=PMC3855844

92. Holmgaard A, Askou AL, Benckendorff JNE, Thomsen EA, Cai Y, Bek T, et al. In Vivo Knockout of the Vegfa Gene by Lentiviral Delivery of CRISPR/Cas9 in Mouse Retinal Pigment Epithelium Cells. Mol Ther - Nucleic Acids [Internet]. 2017 Dec;9(December):89–99. Available from: https://linkinghub.elsevier.com/retrieve/pii/S2162253117302445

93. Izmiryan A, Ganier C, Bovolenta M, Schmitt A, Mavilio F, Hovnanian A. Ex Vivo COL7A1 Correction for Recessive Dystrophic Epidermolysis Bullosa Using CRISPR/Cas9 and Homology-Directed Repair. Mol Ther - Nucleic Acids [Internet]. 2018 Sep;12(September):554–67. Available from: https://doi.org/10.1016/j.omtn.2018.06.008

94. Teng Y, Luo M, Yu T, Chen L, Huang Q, Chen S, et al. CRISPR/Cas9-mediated deletion of miR-146a enhances antiviral response in HIV-1 infected cells. Genes Immun [Internet]. 2019 Apr 2;20(4):327–37. Available from: http://dx.doi.org/10.1038/s41435-018-0036-x

95. Follenzi A, Ailles LE, Bakovic S, Geuna M, Naldini L. Gene transfer by lentiviral vectors is limited by nuclear translocation and rescued by HIV-1 pol sequences. Nat Genet [Internet]. 2000 Jun;25(2):217–22. Available from: http://www.nature.com/articles/ng0600_217

96. Zhang B, Metharom P, Jullie H, Ellem KAO, Cleghorn G, West MJ, et al. The significance of controlled conditions in lentiviral vector titration and in the use of multiplicity of infection (MOI) for predicting gene transfer events. Genet Vaccines Ther. 2004;2:1–10.

97. Logan AC, Nightingale SJ, Haas DL, Cho GJ, Pepper KA, Kohn DB. Factors Influencing the Titer and Infectivity of Lentiviral Vectors. Hum Gene Ther [Internet]. 2004 Oct;15(10):976–88. Available from: http://www.liebertpub.com/doi/10.1089/hum.2004.15.976

98. Tweeddale ME, Lim B, Jamal N, Robinson J, Zalcberg J, Lockwood G, et al. The presence of clonogenic cells in high-grade malignant lymphoma: a prognostic factor. Blood [Internet]. 1987 May;69(5):1307–14. Available from: http://www.ncbi.nlm.nih.gov/pubmed/3567358

99. Jäger V, Büssow K, Wagner A, Weber S, Hust M, Frenzel A, et al. High level transient production of recombinant antibodies and antibody fusion proteins in HEK293 cells. BMC Biotechnol [Internet]. 2013;13(1):52. Available from: http://bmcbiotechnol.biomedcentral.com/articles/10.1186/1472-6750-13-52

100. Pear WS, Nolan GP, Scott ML, Baltimore D. Production of high-titer helper-free retroviruses by transient transfection. Proc Natl Acad Sci U S A [Internet]. 1993 Sep 15;90(18):8392–6. Available from: http://ieeexplore.ieee.org/document/4063626/

101. Hindson BJ, Ness KD, Masquelier DA, Belgrader P, Heredia NJ, Makarewicz AJ, et al. High-Throughput Droplet Digital PCR System for Absolute Quantitation of DNA Copy Number. Anal Chem [Internet]. 2011 Nov 15;83(22):8604–10. Available from: http://www.ncbi.nlm.nih.gov/pubmed/22035192%0Ahttp://www.pubmedcentral.nih.gov/articlerender.fcgi?artid=PMC3216358

102. Popp MW, Maquat LE. Leveraging rules of nonsense-mediated mRNA decay for genome engineering and personalized medicine. Cell [Internet]. 2016;165(6):1319–22. Available from: http://dx.doi.org/10.1016/j.cell.2016.05.053

103. Chang Y-F, Imam JS, Wilkinson MF. The Nonsense-Mediated Decay RNA Surveillance Pathway. Annu Rev Biochem [Internet]. 2007 Jun 7;76(1):51–74. Available from: http://www.annualreviews.org/doi/10.1146/annurev.biochem.76.050106.093909

104. Sharpe JJ, Cooper TA. Unexpected consequences: Exon skipping caused by CRISPR-generated mutations. Genome Biol. 2017;18(1):1240–3.

105. Smith JL, Mou H, Xue W. Understanding and repurposing CRISPR-mediated alternative splicing. Genome Biol. 2018;19(1):184.

106. Sui T, Song Y, Liu Z, Chen M, Deng J, Xu Y, et al. CRISPR-induced exon skipping is dependent on premature termination codon mutations. Genome Biol [Internet]. 2018 Dec 17;19(1):164. Available from: https://genomebiology.biomedcentral.com/articles/10.1186/s13059-018-1532-z

107. Darzynkiewicz Z, Halicka HD, Zhao H. Analysis of cellular DNA content by flow and laser scanning cytometry. Adv Exp Med Biol [Internet]. 2010;676:137–47. Available from: http://www.ncbi.nlm.nih.gov/pubmed/20687474%0Ahttp://www.pubmedcentral.nih.gov/articlerender.fcgi?artid=PMC2967208

108. Qi W, Xie C, Li C, Caldwell JT, Edwards H, Taub JW, et al. CHK1 plays a critical role in the anti-leukemic activity of the wee1 inhibitor MK-1775 in acute myeloid leukemia cells. J Hematol Oncol. 2014;7(1):1–12.

109. Cecchini MJ, Amiri M, Dick FA. Analysis of Cell Cycle Position in Mammalian Cells. J Vis Exp. 2012;(59):1–7.

110. Dolbeare F, Gratzner H, Pallavicini MG, Gray JW. Flow cytometric measurement of total DNA content and incorporated bromodeoxyuridine. Proc Natl Acad Sci [Internet]. 1983 Sep 1;80(18):5573–7. Available from: http://www.ncbi.nlm.nih.gov/pubmed/6577444%0Ahttp://www.pubmedcentral.nih.gov/articlerender.fcgi?artid=PMC384300

111. Falgreen S, Laursen MB, Bødker JS, Kjeldsen MK, Schmitz A, Nyegaard M, et al. Exposure time independent summary statistics for assessment of drug dependent cell line growth inhibition. BMC Bioinformatics [Internet]. 2014 Dec 5;15(1):168. Available from: https://bmcbioinformatics.biomedcentral.com/articles/10.1186/1471-2105-15-168

112. Pesole G, Mignone F, Gissi C, Grillo G, Licciulli F, Liuni S. Structural and functional features of eukaryotic mRNA untranslated regions. Gene [Internet]. 2001 Oct;276(1–2):73–81. Available from: https://linkinghub.elsevier.com/retrieve/pii/S0378111901006746

113. Yu Y, Chen B, Chen Z, Fan C, Han Y, Zhang J, et al. Identification of a novel Wee1 isoform. Biochim Biophys Acta - Gene Struct Expr [Internet]. 2005 May;1729(1):1–9. Available from: https://linkinghub.elsevier.com/retrieve/pii/S0167478105000473

114. Watanabe N. WEE1. In: Choi S, editor. Encyclopedia of Signaling Molecules [Internet]. New York, NY: Springer New York; 2016. p. 1–5. Available from: http://link.springer.com/10.1007/978-1-4614-

6438-9

115. Tomashevski A, Husseman J, Jin L-W, Nochlin D, Vincent I. Constitutive Wee1 activity in adult brain neurons with M phase-type alterations in Alzheimer neurodegeneration. J Alzheimer's Dis [Internet]. 2001 May 14;3(2):195–207. Available from: http://www.medra.org/servlet/aliasResolver?alias=iospress&doi=10.3233/JAD-2001-3205

116. Rajan P, Dalgliesh C, Carling PJ, Buist T, Zhang C, Grellscheid SN, et al. Identification of Novel Androgen-Regulated Pathways and mRNA Isoforms through Genome-Wide Exon-Specific Profiling of the LNCaP Transcriptome. Chan FL, editor. PLoS One [Internet]. 2011 Dec 14;6(12):e29088. Available from: https://dx.plos.org/10.1371/journal.pone.0029088

117. Farrugia MM, Duan LJ, Reis MD, Ngan BY, Berinstein NL. Alterations of the p53 tumor suppressor gene in diffuse large cell lymphomas with translocations of the c-MYC and BCL-2 proto-oncogenes. Blood [Internet]. 1994 Jan 1;83(1):191–8. Available from: http://www.ncbi.nlm.nih.gov/pubmed/8274734

7. Appendix

Supplementary figure 1:

A)

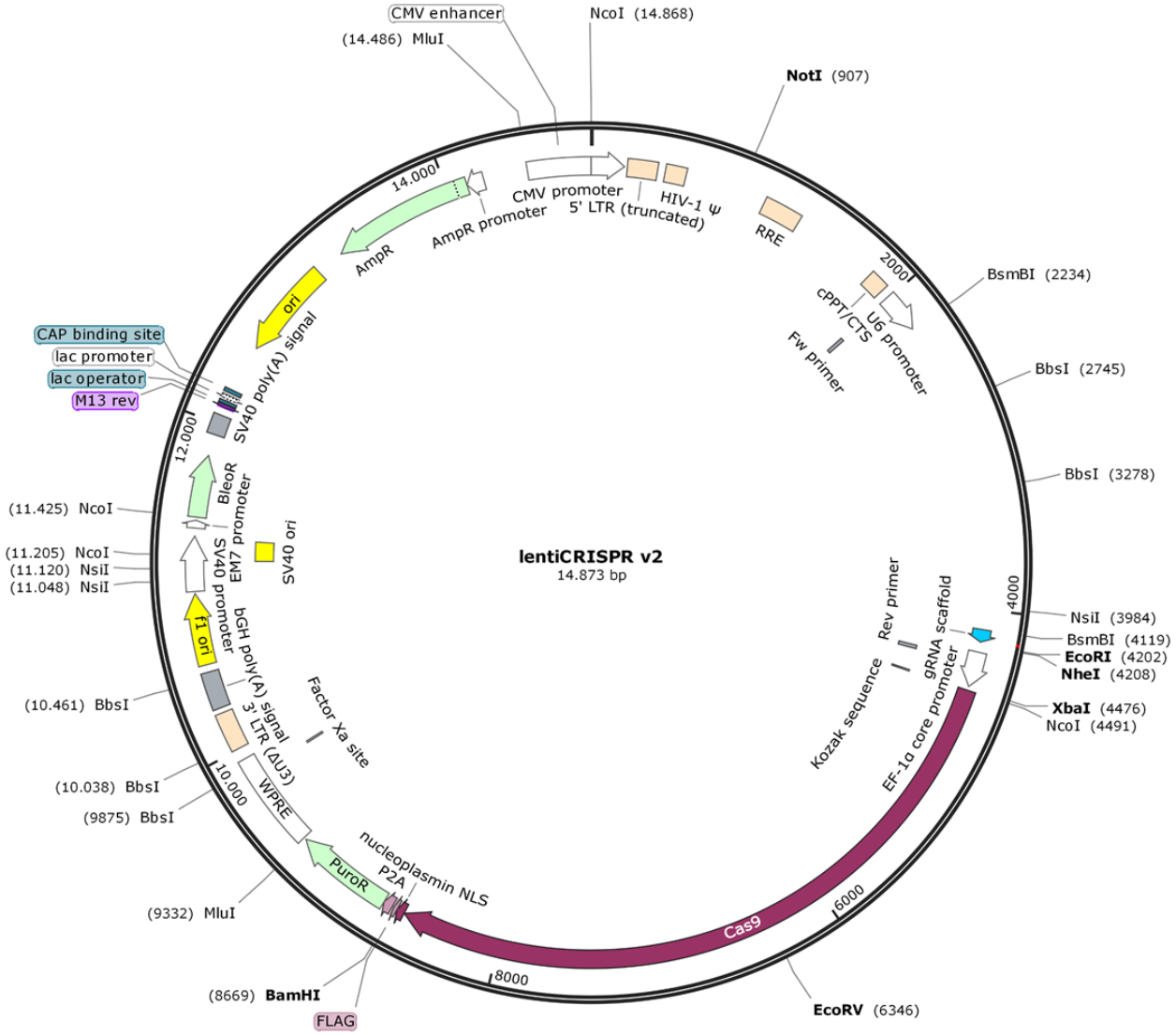

B)

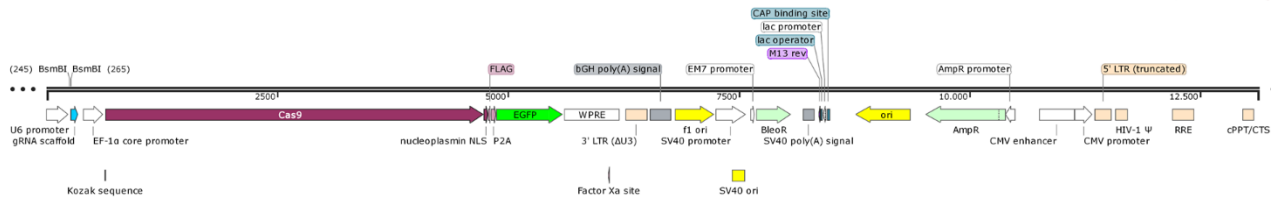

C)

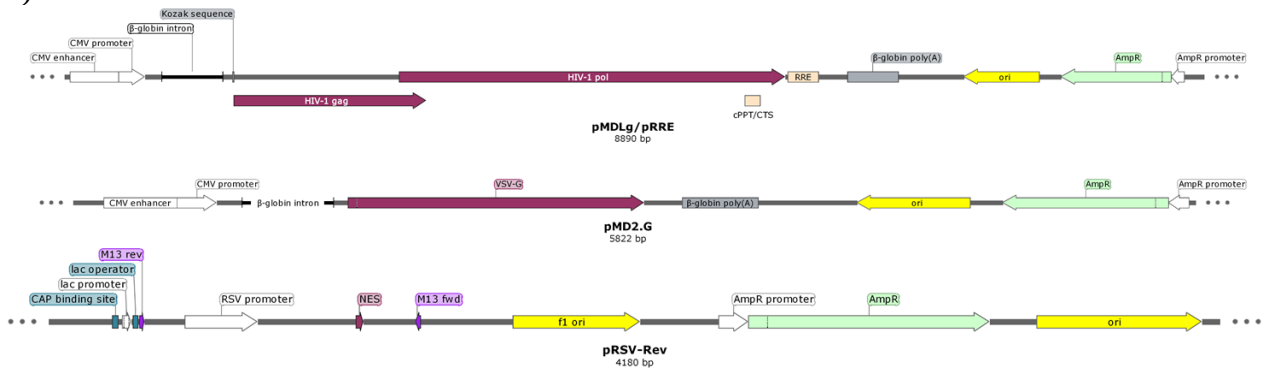

Supplementary figure 1) **Overview of plasmids used in this project**. (**A**) LentiCRISPR v2 was used for cloning and subsequent transfection and is presented with primers and enzyme restriction sites. For cloning BsmBI enzyme was used to insert sgRNAs between position 2,234 and 4,119 in the plasmid. (**B**) lentiCRISPRv2GFP was used for flow cytometry and fluorescence microscopy subsequent to transfection and transduction. (**C**) Lentiviral envelope and packaging plasmids were used for lentiviral production.

Supplementary figure 2:

A)

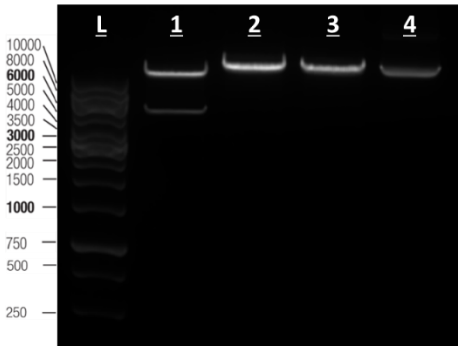

B)

Reagent	Volume
10X NEBuffer 2.1 (NEB, Cat. No.: B7202S)	5 µL
LentiCrispr v2 plasmid (50 ng)	1 ng/µL
NheI *	0.5 µL
BamHI *	0.5 µL
H_2O	To 50 µL

Supplementary figure 2) **Verification of the LentiCRISPR v2 plasmid used throughout the project by enzyme digestion**. (**A**) Gel electrophoresis of the reaction using 1% agarose gel and 1kb ladder. DNA bands after double-digestion using both enzymes produces two DNA fragments of 4,461 bp and 10,412 bp in size (Lane 1), using either enzyme alone produces single bands of the same length (Lanes 2 and 3), and finally the plasmid control with no added enzymes remains supercoiled and therefore looks shorter on the gel. (**B**) The reaction for digestion of the plasmid using NheI and BamHI enzymes. *Reactions were run using either enzyme alone or in combination for digestion.

Supplementary figure 3:

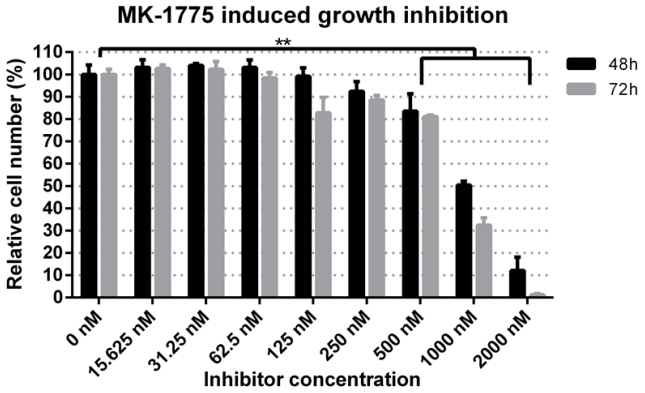

Supplementary figure 3) **Determination of optimal MK-1775 concentration**. 15.6-2000 nM MK-1775 were added to HEK293T WT cells for 48h and 72 h (n=3). Data was assessed for normal distribution and a two-way ANOVA was conducted, comparing each concentration to the treatment control (0 nM). Significant growth inhibition (**P≤0.019) was seen at concentrations higher than 500 nM. Results are presented as mean ± SEM

Supplementary figure 4:

A)

B)

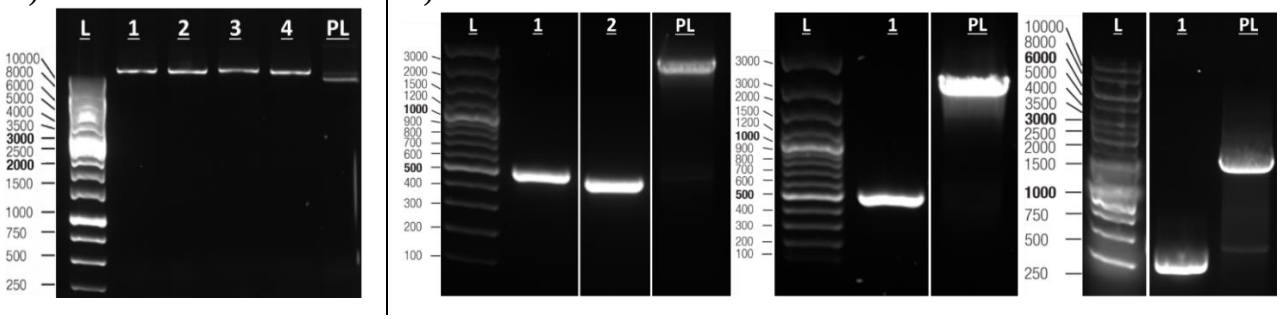

Supplementary figure 4) **Gel electrophoresis showing cloning results of pLv2-sgRNAs**. (**A**) The digestion-ligation product from cloned plasmids pLv2-sgBeta, pLv2-sgGamma, pLv2-sgDelta, and pLv2-sgControl are shown on lanes 1-4 respectively. Here, the negative plasmid control (50 ng LentiCRIPSR v2) has travelled further through the gel due to its supercoiled structure, which also produces a larger smear. Overexposure on this gel barely revealed the excised fragments after cloning. 0.8% agarose gel and an 1kb ladder was used. (**B**) PCR product of pLv2-sgBeta and pLv2-sgGamma (Lanes 1-2 on gel 1), pLv2-sgDelta (Lane 1 on gel 2), and pLv2-sgControl (Lane 1 on gel 3) using primers flanking the sgRNA insertion site subsequent to purification from transformed E.Coli cultures and plasmid purification. Each gel is modified by cutting out negative cloning reactions (indicated by spaces between lanes) and only shows the samples used for further studies. Each gel also included a negative plasmid control. Samples were run through a 1.5 % agarose gel. A 100 bp ladder was used for gels 1-2. A 1 kb ladder was used for gel 3 (due to the curvature of this gel which can be seen in the ladder, the amplicon on lane 1 and PL seem shorter, however the relative distance between lane 1 and PL remains the same as with all positive cloning reactions.

Supplementary figure 5:

A)

Name	Statistic	#Cells
Ly7_transfected A1.fcs		51555
cells	92,4	47643
EGFP+	0,15	76
EGFP-	99,9	51479
Ly7_transfected A2.fcs		98280
Cells	94,2	92604
EGFP+	0,16	155
EGFP-	99,8	98125
Ly7_transfected B1.fcs		52745
Cells	96,6	50939
EGFP+	0,080	42
EGFP-	99,9	52703
Ly7_transfected B2.fcs		100000
Cells	97,2	97174
EGFP+	0,090	90
EGFP-	99,9	99910
Ly7_transfected C1.fcs		100000
Cells	97,9	97912
EGFP+	0,065	65
EGFP-	99,9	99935

Name	Statistic	#Cells
Ly7_transfected C2.fcs		49936
Cells	97,3	48572
EGFP+	0,062	31
EGFP-	99,9	49905
Ly7_transfected D1.fcs		50164
Cells	97,4	48839
EGFP+	0,098	49
EGFP-	99,9	50115
Ly7_transfected D2.fcs		51871
Cells	97,7	50662
EGFP+	0,081	42
EGFP-	99,9	51829
Ly7_untransfected E2.fcs		72310
Cells	98,5	71233
EGFP+	0,069	50
EGFP-	99,9	72260
Ly7_untransfected control E1.fcs		55125
Cells	98,0	54042
EGFP+	0,060	33
EGFP-	99,9	55092

B)

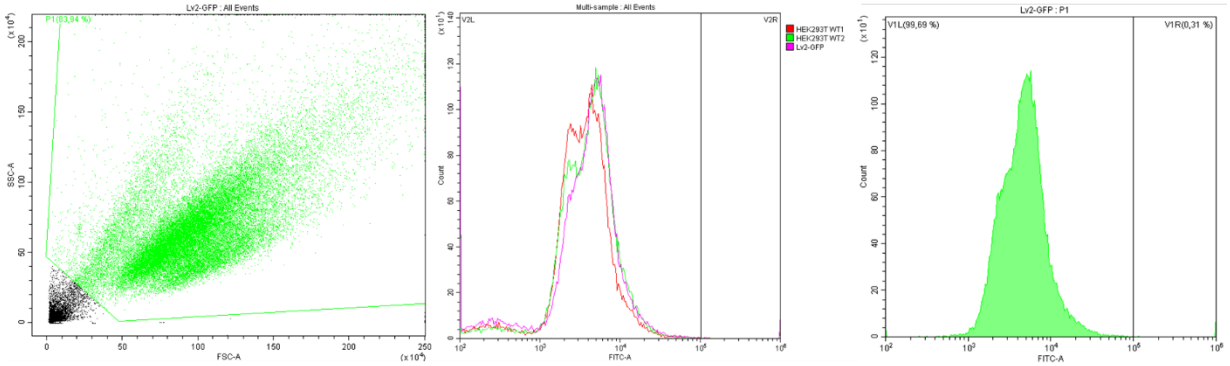

Supplementary figure 5) **Lentiviral transduction of OCI-Ly7 cells**. (**A**) 0.15×10^6, 0.3×10^6 and 0.4×10^6 OCI-Ly7 cells were transduced with 0.5 mL and 1 mL virus-containing supernatant equivalent to 12.2-49 pg p24. eGFP signal was barely detectable and indistinguishable from background noise ($eGFP^+ \leq 0.16\%$, which was ≤155 events) in cell from all wells. (**B**) 1 well containing 0.15×10^6 OCI-Ly7 cells was transduced with ultracentrifuged lentivirus equivalent to 0.83-1.67 ng p24. Cell debris was excluded by gating on forward scatter (FCS-A) and side scatter (SSC) (left). There was no observable difference in eGFP signal between the transduced cells and the two HEK293T WT control cells (middle). By creating a vertical border, transduction efficiency was determined to be 0.31% (right)

Supplementary figure 6:

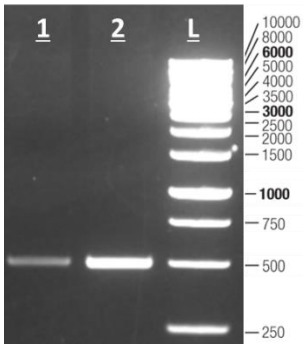

Supplementary figure 6) **PCR on DNA extracted from cells subsequent to puromycin selection.** The presence of plasmids was investigated in HEK293T WT (Lane 1) and the sgDelta transfected cell population (Lane 2) subsequent to puromycin selection by using the plasmid primers previously used to verify cloning. Single bands corresponding to the expected amplicon lengths of the cloned plasmids can be seen in both cell populations, though at a lower intensity on Lane 1. Samples were run through a 1.5 % agarose gel and a 1 kb ladder was used.

Supplementary figure 7:

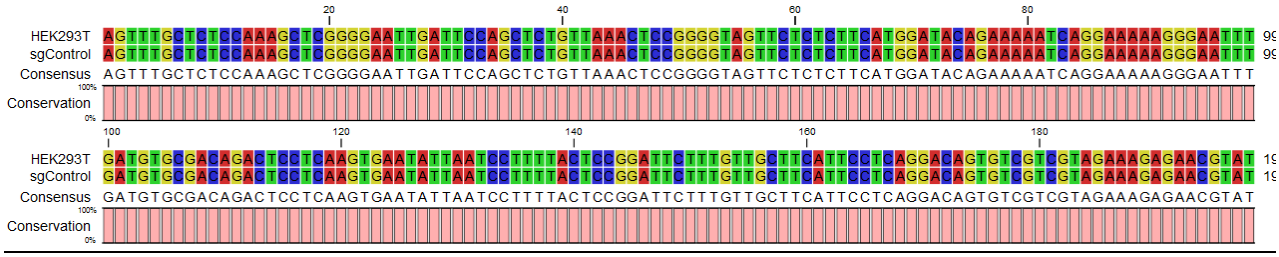

Supplementary figure 7) **Genomic DNA sequence alignment between HEK293T WT cells and sgControl-transfected cell population**. Perfect alignment was seen in the region spanning the target sites for all four sgRNAs used, validating sgControl as a negative control for indel analysis.

Supplementary figure 8:

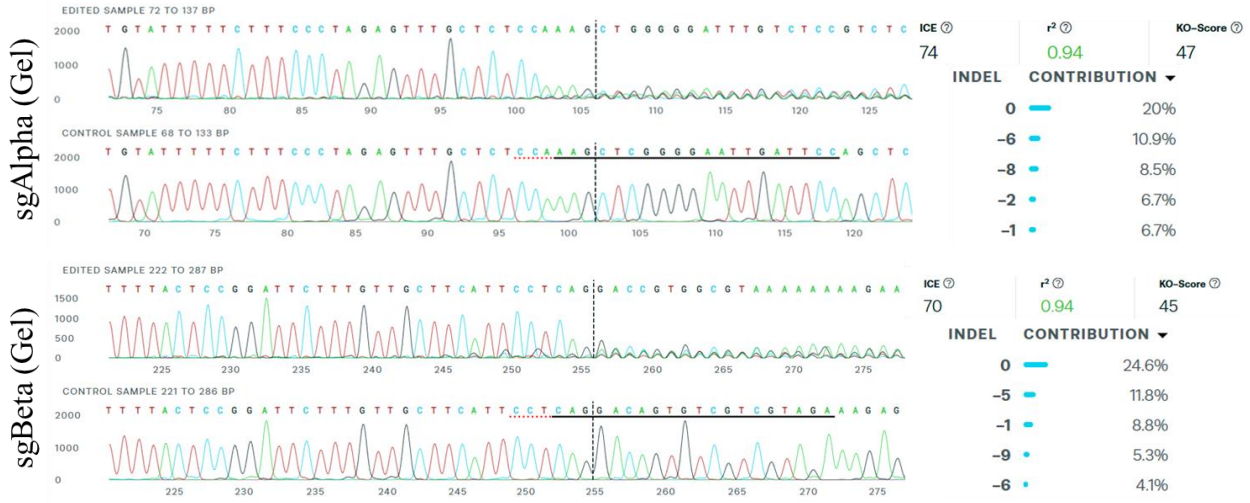

Supplementary figure 8) **Indel analysis of sgRNAs targeting Wee1 using amplicons purified from gels.** The ICE tool was used to analyze the indel formation of cells transfected with pLv2-sgAlpha and pLv2-sgBeta. Subsequent to puromycin selection, a region surrounding the CRISPR/Cas9 target sites on Wee1 was PCR amplified, amplicons purified directly, and Sanger sequenced. Sequencing chromatograms displayed mixed signals with low amplitudes in the region surrounding the Cas9 cut site and downstream indicating that various indel mutations was formed, thus making the cell populations highly heterogenous. DNA bases shown on top are from the most prominent peaks on chromatograms. Examination of the top 5 indels revealed that mutations mainly consisted of deletions. Quantification of sequencing chromatograms using the ICE tool showed high Indel percentages of 70% and 74%, and knockout scores of 45% and 47%.

Supplementary figure 9:

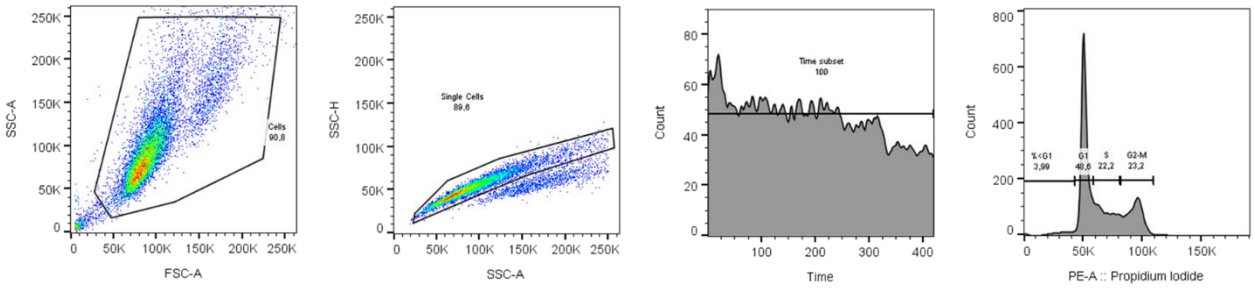

Supplementary figure 9) **Gating strategy for cells used in cell cycle analysis.** First, cell debris was excluded by gating on forward scatter (FCS-A) and side scatter (SSC) (Left). Next, doublet discrimination was performed for to only include single cells in the analysis. Cells were then assessed by gating on time, as all liquid was used in the analysis. Lastly, cell cycle phases were determined by manual gating on the PE-A channel (Left). Cells in the G1 and G2/M phases were initially determined based the peaks, followed by determination of sub-G1 and S phase cells.

Supplementary figure 10:

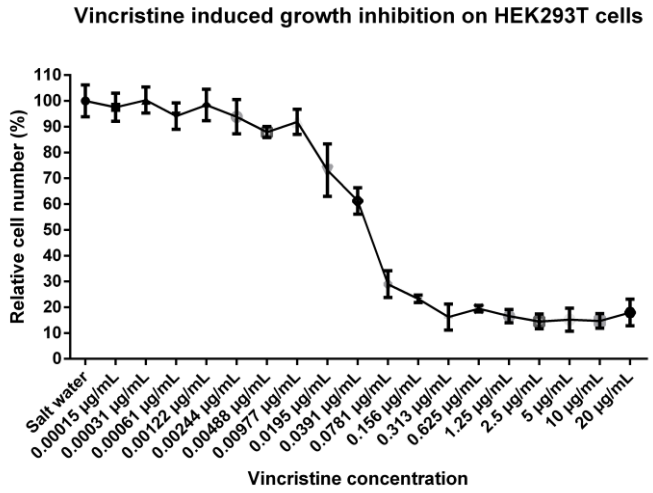

Supplementary figure 10) A large range of vincristine concentrations were tested on HEK293T WT cells prior to dose-response assays on cells transfected with Wee1 targeting sgRNAs. Results are presented as mean ± SEM

Supplementary figure 11:

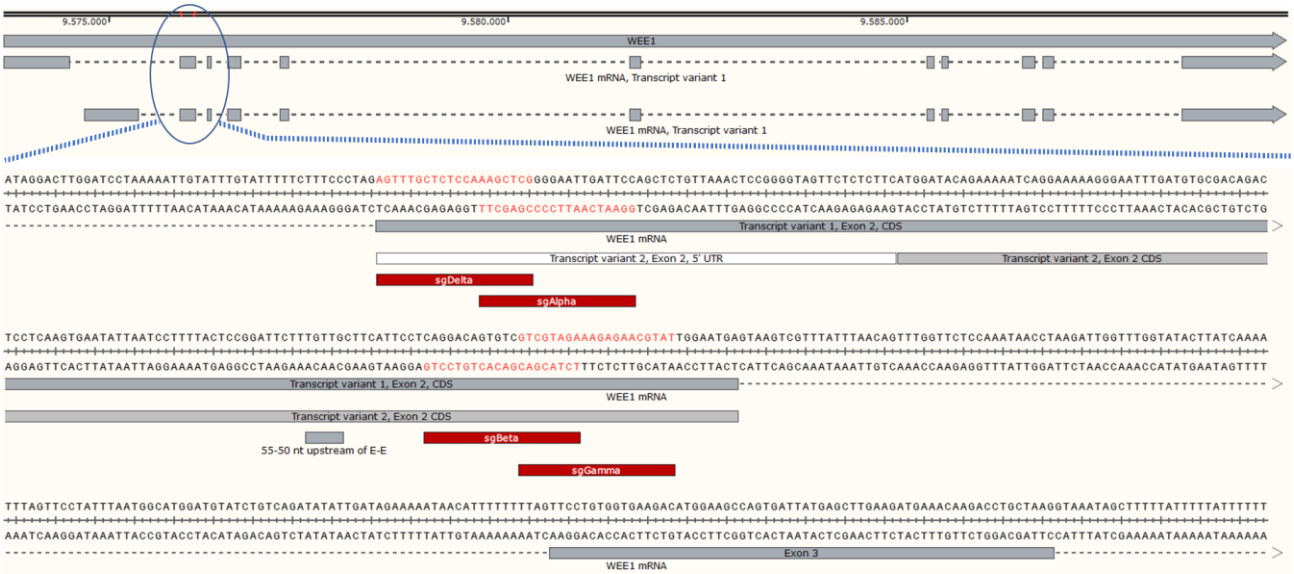

Supplementary figure 11) **Overview of Wee1 gene, and a zoomed in section of the DNA sequence of exon 2-exon 3.** Included are the target sites for each sgRNA (Red text and boxes) and the protein coding regions (CDS) for both transcripts on exon 2 (Grey boxes), the 5' untranslated region (UTR) for transcript 2 on exon 2, and a marker of the region 50-55 nt upstream of exon 2-exon 3 junction. Image was generated using the SnapGene software (GSL Biotech)

Supplementary table 1:

Primers and probes	**Primer sequences and assay ID**	**Target sites and product sizes**
LentiCRISPR v2 primers (plasmid)	F: 5'- CCGAGGGCCTATTTCCCATGATTC -3' R: 5'- TTCTCTAGGCACCGGATCAATTGC -3'	**Target:** 251 bp upstream of first BsmBI restriction site (on the U6 promoter), and 212 bp downstream of second BsmBI restriction site (on sgRNA scaffold). **Product size**: 483-484 bp or 2,344 bp*
WEE1, exon 2 (gDNA)	F: 5' - GTGTGTTGCTTTCACCTACGC - 3' R: 5' - ATACTCATCAACAGAGCCCGC- 3'	**Target**: Wee1, exon 2 (NC_000011.10) **Product size**: 893 bp
WEE1 probe, FAM	Assay ID: Hs01119390_g1	**Target**: Wee1 mRNA (Exon boundary 8 – 9) **Product size**: 86 bp
TBP probe, FAM	Assay ID: Hs00427620_m1	**Target**: TATA-box binding protein mRNA (exon boundary 2-3 on NM_001172085.1 and exon boundary 3-4 on NM_003194.4) **Product size**: 91 bp

Supplementary table 1) **Table of primers and probes used throughout this project**. *primers targeting LentiCRISPR v2 varies in the amplicon size depending on whether the plasmids are used for cloning (and sgRNAs are inserted) or not. The same primers were used for both PCR and sequencing of plasmids. F = Forward primer, R = Reverse primer.